NUREG/CR-5704
ANL-98/31

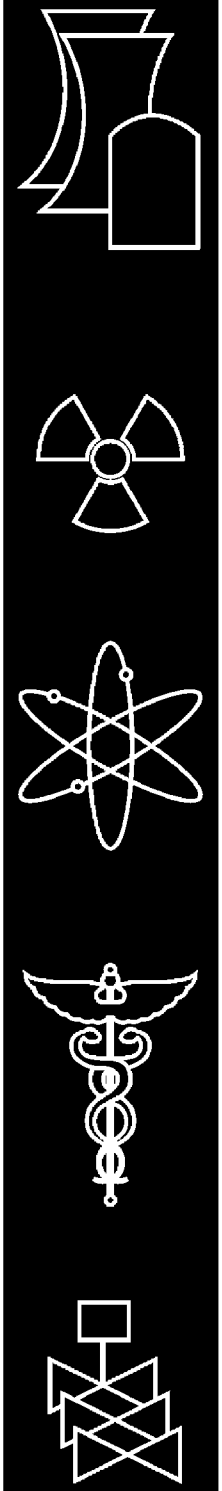

Effects of LWR Coolant Environments on Fatigue Design Curves of Austenitic Stainless Steels

Argonne National Laboratory

U.S. Nuclear Regulatory Commission
Office of Nuclear Regulatory Research
Washington, DC 20555-0001

NUREG/CR-5704
ANL-98/31

Effects of LWR Coolant Environments on Fatigue Design Curves of Austenitic Stainless Steels

Manuscript Completed: November 1998
Date Published: April 1999

Prepared by
O. K. Chopra

Argonne National Laboratory
9700 South Cass Avenue
Argonne, IL 60439

M. McNeil, NRC Project Manager

Prepared for
Division of Engineering Technology
Office of Nuclear Regulatory Research
U.S. Nuclear Regulatory Commission
Washington, DC 20555-0001
NRC Job Code W6610

EFFECTS OF LWR COOLANT ENVIRONMENTS ON FATIGUE DESIGN CURVES OF AUSTENITIC STAINLESS STEELS

by

O. K. Chopra

Abstract

The ASME Boiler and Pressure Vessel Code provides rules for the construction of nuclear power plant components. Figures I–9.1 through I–9.6 of Appendix I to Section III of the Code specify fatigue design curves for structural materials. While effects of reactor coolant environments are not explicitly addressed by the design curves, test data indicate that the Code fatigue curves may not always be adequate in coolant environments. This report summarizes work performed by Argonne National Laboratory on fatigue of austenitic stainless steels in light water reactor (LWR) environments. The existing fatigue S–N data have been evaluated to establish the effects of various material and loading variables such as steel type, dissolved oxygen level, strain range, strain rate, and temperature on the fatigue lives of these steels. Statistical models are presented for estimating the fatigue S–N curves as a function of material, loading, and environmental variables. Design fatigue curves have been developed for austenitic stainless steel components in LWR environments. The extent of conservatism in the design fatigue curves and an alternative method for incorporating the effects of LWR coolant environments into the ASME Code fatigue evaluations are discussed.

Contents

Figures

Tables

Executive Summary

Section III, Subsection NB of the ASME Boiler and Pressure Vessel Code contains rules for the design of Class 1 components. Figures I–9.1 through I–9.6 of Appendix I to Section III specify the Code design fatigue curves for applicable structural materials. However, Section III, Subsection NB–3121 of the Code states that effects of the coolant environment on fatigue resistance of a material were not intended to be addressed in these design curves. Therefore, there is uncertainty about the effects of environment on fatigue resistance of materials used in operating pressurized water reactor (PWR) and boiling water reactor (BWR) plants, whose primary–coolant–pressure–boundary components were designed in accordance with the Code.

The current Section–III design fatigue curves of the ASME Code were based primarily on strain–controlled fatigue tests of small polished specimens at room temperature in air. Best–fit curves to the experimental test data on stress or on cycles, were lowered by a factor of 2 on stress or 20 on cycles, whichever was more conservative, to obtain the design fatigue curves. These factors are not safety margins but rather adjustment factors that must be applied to experimental data to obtain estimates of the lives of components. They were not intended to address the effects of the coolant environment on fatigue life. Recent fatigue strain vs. life (S–N) data obtained in the U.S. and Japan demonstrate that light water reactor (LWR) environments can have potentially significant effects on the fatigue resistance of materials. Specimen lives obtained from tests in simulated LWR environments can be much shorter than those obtained from corresponding tests in air.

This report summarizes work performed by Argonne National Laboratory on fatigue of austenitic stainless steels (SSs) in simulated LWR environments. The existing fatigue S–N data, foreign and domestic, for wrought and cast stainless steels have been evaluated to establish the effects of various material and loading variables on fatigue life. Statistical methods have been used to develop fatigue S–N curves that include the effects of material, loading, and environmental variables. An alternative method for incorporating the effects of LWR coolant environments into the ASME Code fatigue design curves is presented.

Overview of Fatigue S–N Data

In air, the fatigue lives of Types 304 and 316 SS are comparable; those of Type 316NG are superior. The fatigue S–N behavior of cast CF–8 and CF–8M SSs is similar to that of wrought austenitic SSs. The fatigue life of all steels is independent of temperature in the range from room temperature to 427°C; at temperatures above 260°C, it may decrease with decreasing strain rate. The ASME mean curve for austenitic SSs is nonconservative with respect to the existing fatigue S–N data; at strain amplitudes <0.5%, the mean curve predicts significantly longer fatigue lives than those observed experimentally.

The fatigue lives of cast and wrought austenitic SSs is decreased in LWR environments. The reduction in life depends on strain rate, dissolved oxygen (DO) level in water, and temperature. The effect of LWR environments on fatigue life is comparable for all steels. The results indicate that a minimum threshold strain is required to produce an environmentally assisted decrease in the fatigue life of these steels. The threshold value most likely corresponds to the rupture strain of the surface oxide film; limited data suggest that the threshold strain is between 0.32 and 0.36%.

The effects of environment on fatigue life occur primarily during the tensile–loading cycle, and at strain levels greater than the threshold value required to rupture the surface oxide film. Consequently, loading and environmental conditions, e.g., strain rate, temperature, and DO level, in excess of the oxide rupture strain during the tensile–loading cycle, are important parameters for environmentally assisted reduction of fatigue life of these steels. Unlike ferritic steels, where environmental effects are greater in high–DO environments, environmental effects on fatigue life of austenitic stainless steels are more pronounced in low– than in high–DO water. The reduction in life is greater by a factor of ≈2 in simulated PWR environment, i.e., <0.01 ppm DO, than in high–DO water, i.e., ≥0.1 ppm DO. Existing data are inadequate to establish the functional form for the dependence of fatigue life on DO content. Recent data indicate that conductivity of water is important for environmental effects on fatigue life in high–DO water. The fatigue lives of cast SSs are approximately the same in both high– and low–DO water and are comparable to those observed for wrought SSs in low–DO water.

The fatigue lives of austenitic SSs decrease with decreasing strain rate; the effect is greater in a low–DO PWR environment than in high–DO water. The results indicate that the rate below which the effects of strain rate on fatigue life saturate may depend on both steel type and DO level. In low–DO PWR environments, saturation strain rate appears to be at ≈0.0004%/s for Type 304 SS and somewhat higher for Type 316 SS. The existing data are inadequate to establish the functional form for the dependence of life on temperature. Limited data indicate that environmental effects on fatigue life are significant at 250°C and minimal below 200°C.

Fatigue Design Curves in LWR Environments

Statistical models have been developed to predict fatigue lives of small smooth specimens of austenitic SSs as a function of material, loading, and environmental parameters. The functional form and bounding values of these parameters were based on experimental observations and data trends. The statistical models were obtained by minimizing the squared Cartesian distances from the data point to the predicted curve instead of minimizing the sum of the square of the residual errors for either strain amplitude or fatigue life. The models are recommended for predicted fatigue lives $\leq 10^6$ cycles. The results indicate that the ASME mean curve for SSs is not consistent with the experimental data at strain amplitudes <0.5% or stress amplitudes <975 MPa (<141 ksi); the ASME mean curve is non conservative.

The design fatigue curves for austenitic SSs in LWR environments were obtained by the procedure that has been used to develop the current ASME Code design fatigue curves, i.e., by adjusting the best–fit experimental curve for the effect of mean stress and setting margins of 20 on cycles and 2 on strain to account for the uncertainties in life that are associated with material and loading conditions. However, because the margin on strain for the current ASME Code design fatigue curve is closer to 1.5 than 2, a factor of 1.5 was used in developing the design fatigue curves for LWR environments. Data available in the literature were reviewed to evaluate the conservatism in the existing Code fatigue design curves. The use of a fatigue life correction factor to incorporate the effects of environment into the ASME Code fatigue evaluations is also discussed.

Acknowledgments

The author thanks J. L. Smith, W. F. Burke, T. M. Galvin, and J. Tezak for their contributions to the experimental effort and W. J. Shack and T. F. Kassner for helpful discussions. This work is sponsored by the Office of Nuclear Regulatory Research, U.S. Nuclear Regulatory Commission, under Job Code W6610-6; Program Manager: Dr. M. B. McNeil.

1 Introduction

Experience with operating nuclear power plants worldwide reveals that many failures, e.g., in piping components, nozzles, valves, and pumps, may be attributed to fatigue.[1–3] In most cases, these failures have been associated with thermal loading due to thermal stratification or thermal striping, or with mechanical loading due to vibration. Significant thermal loadings due to flow stratification were not included in the original design basis analysis. The effect of these loadings may also have been aggravated by corrosion effects due to exposure to high–temperature aqueous environments. Fatigue cracks have been observed in pressurizer surge lines in pressurized water reactors (PWRs) (NRC Bulletin No. 88–11), and in feedwater lines connected to nozzles of pressure vessels in boiling water reactors (BWRs) and steam generators in PWRs (NRC IE Bulletin, 79–13; NRC Information Notice 93–20). These cracks have been attributed to corrosion fatigue (NRC IE Bulletin, 79–13) or strain–induced corrosion cracking[4] caused by cyclic loading due to thermal stratification during startup (hot standby) and shutdown periods.

Cyclic loadings on a structural component occur because of changes in the mechanical and thermal loadings as the system goes from one set of pressure, temperature, moment, and force loading to any other load set. For each pair of load sets, an individual fatigue usage factor is determined by the ratio of the number of cycles anticipated during the lifetime of the component to the allowable cycles. Figures I–9.1 through I-9.6 of Appendix I to Section III of the ASME Boiler and Pressure Vessel Code[5] specifies fatigue design curves that define the allowable number of cycles as a function of applied stress amplitude. The cumulative usage factor (CUF) is the sum of the individual usage factors, and Section III of the ASME Code requires that the CUF at each location must not exceed 1.

The Code design fatigue curves were based on strain–controlled tests of small polished specimens at room temperature in air. In most studies, the fatigue life of a test specimen is defined as the number of cycles required for the tensile stress to drop 25% from its peak value. Such a drop corresponds to an ≈3–mm–deep crack. Consequently, fatigue life N represents the number of cycles required to initiate a crack ≈3 mm deep. The best–fit curves to the experimental data were expressed in terms of the Langer equation[6] of the form

$$\varepsilon_a = B(N)^{-b} + A, \qquad (1)$$

where A, B, and b are parameters of the model. Equation 1 may be written in terms of stress amplitude S_a instead of strain amplitude ε_a, in which case stress amplitude is the product of strain amplitude and elastic modulus, i.e., $S_a = E_a.\varepsilon$ The design fatigue curves were obtained by decreasing the best–fit curves by a factor of 2 on stress or 20 on cycles, whichever was more conservative, at each point on the best–fit curve. As described in the ASME Section–III criteria document, these factors were intended to account for the differences and uncertainties in relating the fatigue lives of laboratory test specimens to those of actual reactor components. The factor of 20 on cycles is the product of three separate subfactors: 2 for scatter of data (minimum to mean), 2.5 for size effects, and 4 for surface finish, atmosphere, etc. “Atmosphere” was intended to reflect the effects of an industrial environment rather than the controlled environment of a laboratory. The factors of 2 and 20 are not safety margins but rather conversion factors that must be applied to the experimental data to obtain reasonable

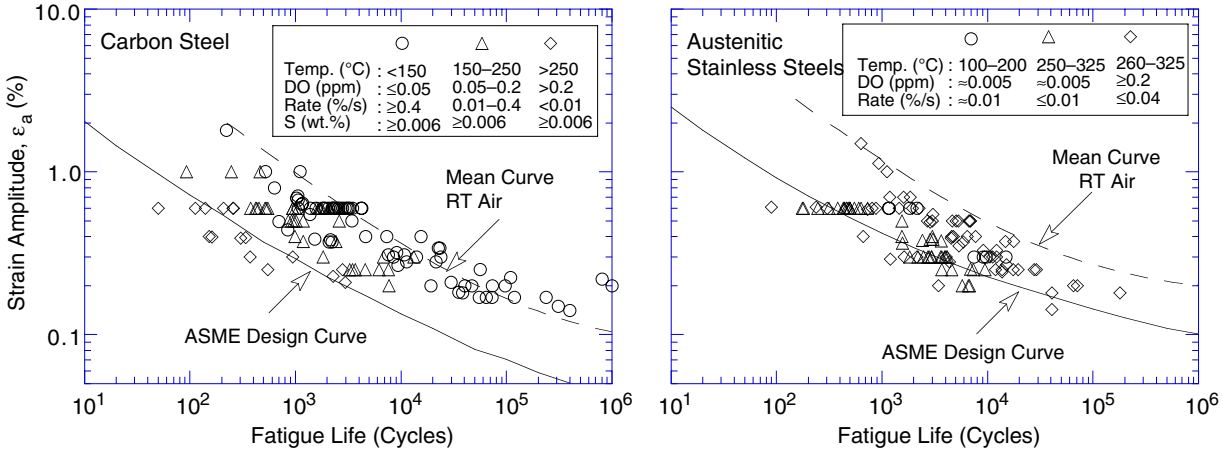

Figure 1. Fatigue S–N data for CSs and austenitic SSs in water (RT = room temperature)

estimates of the lives of actual reactor components. In a benign environment, some fraction of the factors actually represents a safety margin.

Subsection NB–3121 of Section III of the Code states that the data on which the fatigue design curves (Figs. I–9.1 through I–9.6) are based did not include tests in the presence of corrosive environments that might accelerate fatigue failure. Article B–2131 in Appendix B to Section III states that the owner's design specifications should provide information about any reduction to fatigue design curves that is required because of environmental conditions. Recent fatigue strain–vs.–life (S–N) data illustrate potentially significant effects of light water reactor (LWR) coolant environments on the fatigue resistance of carbon steels (CSs) and low–alloy steels (LASs),[7–20] as well as of austenitic stainless steels (SSs),[21–31] (Fig. 1). Under certain conditions of loading and environment, fatigue lives of CSs can be a factor of 70 lower in the environment than in air.[10,17–20] Therefore, the margins in the ASME Code may be less conservative than originally intended.

A program is being conducted at Argonne National Laboratory (ANL) to develop data and models for predicting the effects of environment on fatigue design curves of pressure vessel and piping steels and to assess the additivity of fatigue damage under load histories typical of LWR components. Fatigue tests are being conducted to establish the effects of various loading and environmental variables on the fatigue S–N behavior of pressure boundary steels. Interim design fatigue curves that address environmental effects on fatigue life of carbon and low–alloy steels and austenitic SSs have been proposed; they are based on existing fatigue S–N data.[32] Statistical models have also been developed at ANL for estimating the effects of various material and loading conditions on the fatigue life of these materials.[33,34] Results of the statistical analysis have been used to estimate the probability of fatigue cracking in reactor components. The statistical models for carbon and low–alloy steels have recently been updated with a larger fatigue S–N data base.[18–20]

The interim design curve and statistical model for austenitic SSs were based on limited data. For example, nearly all of the data in water were obtained at high temperatures (280–320°C) and high levels of dissolved oxygen (DO) (0.2–8 ppm). The data were inadequate to define the loading and environmental conditions that can decrease fatigue life of austenitic SSs. The threshold for strain amplitude above which environment can decrease fatigue life, and the value of strain rate below which environmental effects saturate, were based on the data for carbon and low–alloy steels. Fatigue lives in LWR environments were assumed to be independent of temperature. Furthermore, although the proposed interim fatigue design curve[33,34] for austenitic SSs was based on data

obtained in high–DO water, the curve was recommended for use at all oxygen levels until additional data became available, on the assumption that this was a conservative estimate of the likely effect of DO. Recent experimental results indicate that this assumption is not true.[29–31] Also, the effects of LWR environments on the fatigue lives of cast SSs have not been addressed. Recent test results and a larger fatigue S–N data base have led to the update of statistical models that were developed earlier for estimating the fatigue lives of austenitic SSs in LWR environments.[31]

This report summarizes available data on the effects of various material and loading variables, such as steel type, DO level, strain range, and strain rate, on the fatigue lives of wrought and cast austenitic SSs. The data have been analyzed to identify key parameters that influence fatigue life and define the threshold and saturation values of these parameters. The updated statistical models for estimating the fatigue lives of austenitic SSs in LWR environments are presented. The significance of the effect of environment on the current Code design curve is evaluated.

2 Experimental

Fatigue tests have been conducted on Types 316NG and 304 SS and two heats of CF–8M cast SS to establish the effects of LWR coolant environments on fatigue lives of these steels. The chemical composition of the steels is given in Table 1. For the CF–8M steels, fatigue specimens were obtained from material that was thermally aged for 10,000 h at 400°C; Heat 74 was tested both in the unaged and aged condition. Smooth cylindrical specimens with 9.5–mm diameter and 19–mm gauge length were used for the fatigue tests (Fig. 2). A 1–μm surface finish in the axial direction on the specimen gauge length to prevent circumferential scratches that might act as sites for crack initiation.

Table 1. Composition (in wt.%) of wrought and cast SSs used for fatigue tests

Material	Heat	Source	C	P	S	Si	Cr	Ni	Mn	Mo	Cu	N
Type 316NG[a]	D432804	Vendor	0.011	0.020	0.001	0.52	17.55	13.00	1.76	2.49	0.10	0.108
		ANL	0.013	0.020	0.002	0.49	17.54	13.69	1.69	2.45	0.10	0.105
Type 304[b]	30956	Vendor	0.060	0.019	0.007	0.48	18.99	8.00	1.54	0.44	–	0.100
CF–8M [c]	74	ANL	0.064	–	–	0.73	19.11	9.03	0.54	2.51	–	0.048
CF–8M [d]	75	ANL	0.065	–	–	0.67	20.86	9.12	0.53	2.58	–	0.052

[a]ASME SA312 seamless stainless steel pipe (hot–finished), 610–mm O.D. and 30.9–mm wall, fabricated by Sumitomo Metal Industries, Ltd. Solution-annealed at 1038–1093°C for 0.5 h and water-quenched.
[b]Solution-annealed at 1050°C for 0.5 h.
[c]Solutionannealed 1065–1120°C and waterquenched, measured ferrite content 18%.
[d]Solutionannealed 1065–1120°C and waterquenched, measured ferrite content 28%.

Tests in water were conducted in a small autoclave with an annular volume of 12 mL; see Fig. 3. The once–through system consists of a 132–L supply tank, Pulsafeeder™ pump, heat exchanger, preheater, and autoclave. Water is circulated at a rate of ≈10 mL/min and a system pressure of 9 MPa. The autoclave is constructed of Type 316 SS and contains a titanium liner. The supply tank and most of the low–temperature piping are Type 304 SS;

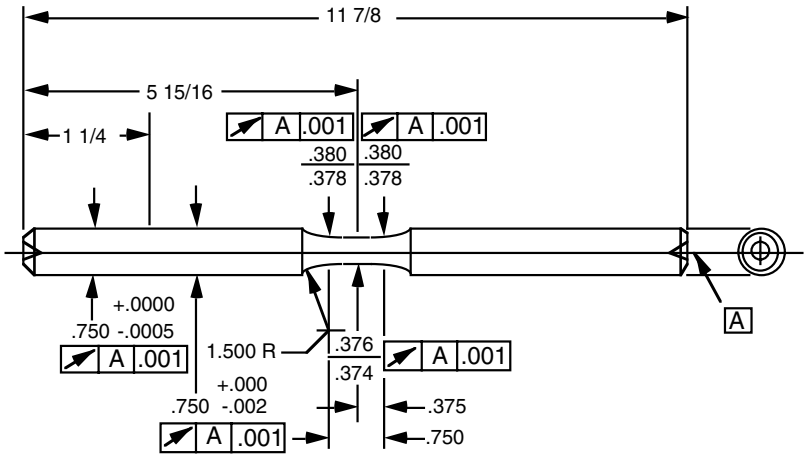

Figure 2. Configuration of fatigue test specimen (all dimensions in inches)

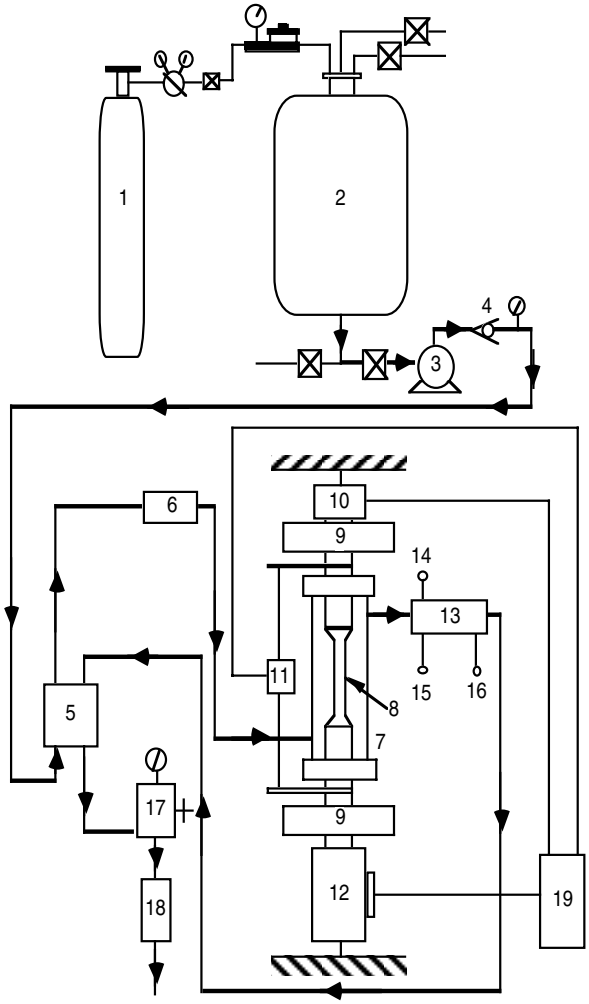

1. Cover–gas supply tank
2. Water supply tank
3. Pulsafeeder high–pressure pump
4. Check valve
5. Heat exchanger
6. Preheat exchanger
7. Pipe autoclave
8. Fatigue test specimen
9. MTS hydraulic collet grips
10. MTS load cell
11. Displacement LVDT
12. MTS hydraulic actuator
13. ECP cell
14. Platinum electrode
15. Specimen electrode
16. Reference electrode
17. Mity Mite™ back–pressure regulator
18. Orbisphere dissolved–oxygen meter
19. MTS electrohydraulic controls

Figure 3. Schematic diagram of autoclave system for fatigue tests in water environment

titanium tubing is used in the heat exchanger and for connections to the autoclave and electrochemical potential (ECP) cell. An Orbisphere meter and CHEMetrics™ ampules were used to measure the DO concentrations in the supply and effluent water. The redox and open–circuit

corrosion potentials were monitored at the autoclave outlet by measuring the ECPs of platinum and an electrode of the test material, respectively, against a 0.1–M KCl/AgCl/Ag external (cold) reference electrode. The measured ECPs, $E_{(meas)}$ (mV), were converted to the standard hydrogen electrode (SHE) scale, $E_{(SHE)}$ (mV), by the polynomial expression[35]

$$E_{(SHE)} = E_{(meas)} + 286.637 - 1.0032(\Delta T) + 1.7447x10^{-4}(\Delta T)^2 - 3.03004x10^{-6}(\Delta T)^3, \quad (2)$$

where ΔT (°C) is the test temperature of the salt bridge in the reference electrode minus the ambient temperature. The test facility was later modified from a once–through system to a recirculating system. For fatigue tests in high–DO environments, an ion–exchange filter was added to the return line to maintain the high resistivity of the water. Also, a filter was installed in the cover–gas line to eliminate possible contamination. A similar recirculating system was used for fatigue tests in simulated low–DO PWR environments, except that the ECP cell was bypassed during recirculation and the ion–exchange filter in the return line from the autoclave to the feedwater supply tank was excluded.

After an initial transition period, when an oxide film develops on the fatigue sample, the DO level and ECP remain constant during the fatigue tests in either the once–through or recirculating water system. Although the difference between the DO levels in the feedwater and effluent water is >0.1 ppm, the difference between the DO levels at the inlet and outlet of the autoclave is ≈0.02 ppm.

The DO level in the water was established by bubbling nitrogen that contains 1–2% oxygen through deionized water in the supply tank. The deionized water was prepared by passing purified water through a set of filters that comprise a carbon filter, an Organex–Q filter, two ion exchangers, and a 0.2–mm capsule filter. Water samples were taken periodically to measure pH, resistivity, and DO concentration. When the desired concentration of DO was attained, the nitrogen/oxygen gas mixture in the supply tank was maintained at a 20–kPa overpressure. After an initial transition period during which an oxide film develops on the fatigue specimen, the DO level and the ECP in the effluent water remained constant during the test. Test conditions are described in terms of the DO in effluent water.

Simulated PWR water was obtained by dissolving boric acid and lithium hydroxide in 20 L of deionized water before adding the solution to the supply tank. The DO in the deionized water was reduced to <10 ppb by bubbling nitrogen through the water. A vacuum was drawn on the tank cover gas to speed deoxygenation. After the DO was reduced to the desired level, a 34–kPa overpressure of hydrogen was maintained to provide ≈2 ppm dissolved hydrogen (or ≈23 cm^3/kg) in the feedwater.

All tests were conducted at 288°C, with fully reversed axial loading (i.e., R = –1) and a triangular or sawtooth waveform. The tests in water were performed under stroke control, wherein the specimen strain was controlled between two locations outside the autoclave. Tests in air were performed under strain control with an axial extensometer; the stroke at the location used to control the water tests was also recorded. Information from the air tests was

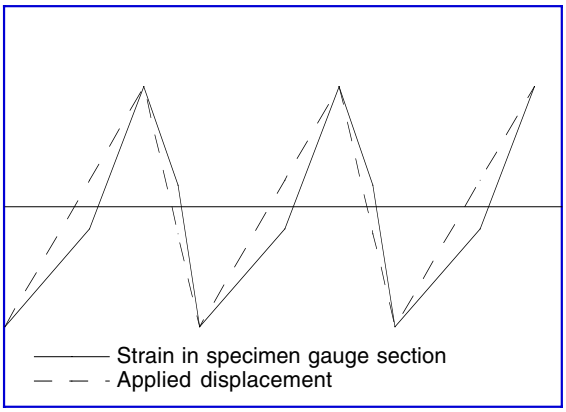

Figure 4.
Total applied displacement (dashed line) and strain in specimen gauge section (solid line) during stroke–controlled tests with a sawtooth waveform

used to determine the stroke required to maintain constant strain in the specimen gauge. To account for cyclic hardening of the material, the stroke that was needed to maintain constant strain was gradually increased during the test. Figure 4 shows the actual strain in the specimen gauge section during a stroke–controlled test with a sawtooth waveform. The fraction of applied displacement that goes to the specimen gauge section is not constant but varies with loading strain. Consequently, the loading rate also varies during the fatigue cycle; it is lower than the applied strain rate at strain levels below the elastic limit and higher at larger strains.

The strain–controlled fatigue tests in air on cast SS specimens showed strain ratcheting in compression. Although strain in the gauge section of the specimens remained constant, overall length of the specimens decreased during the test. The results indicated that strain ratcheting was caused by differences in the strain hardening behavior of these steels in tension and compression. For both heats of CF–8M steel, strain hardening was greater in compression than in tension. The result of this difference was a mean compressive stress, which caused strain ratcheting of the shoulder region of the specimens. To prevent strain racheting, tests in water were conducted under stroke control with a small tensile strain.

To date, the fatigue results obtained on Types 316NG and 304 SS and two heats of CF–8M cast SS in air and LWR environments are summarized in Tables 2–4. The fatigue life N_{25} is defined as the number of cycles for tensile stress to drop 25% from its peak value. Fatigue lives defined by other criteria, e.g., a 50% decrease in peak tensile stress or complete failure, may be converted to an N_{25} value by solving the equation

$$N_{25} = N_X / (0.947 + 0.00212\ X), \qquad (3)$$

where X is the failure criteria, i.e., 25, 50, or 100% decrease in peak tensile stress. For tests in water, the DO level and ECPs of platinum and SS electrodes represent the values in the effluent, and the pH and conductivity of water were both measured in the supply tank.

Table 2. Fatigue test results for Type 316NG austenitic SS

Test No.	Env.[a]	DO[b] (ppb)	pH at RT	Conductivity [c] (µS/cm)	ECP Pt mV (SHE)	ECP Steel mV (SHE)	Ten. Rate (%/s)	Comp. Rate (%/s)	Stress Range (MPa)	Strain Range (%)	Life N_{25} (Cycles)
Room Temp.											
1394	Air	–	–	–	–	–	5.0E-1	5.0E-1	694.7	1.51	4,649
1391	Air	–	–	–	–	–	5.0E-1	5.0E-1	554.8	1.00	13,561
1390	Air	–	–	–	–	–	5.0E-1	5.0E-1	518.1	0.75	25,736
1396	Air	–	–	–	–	–	5.0E-1	5.0E-1	506.7	0.76	30,000
1420	Air	–	–	–	–	–	4.9E-1	4.9E-1	495.3	0.49	54,249
1392	Air	–	–	–	–	–	5.0E-1	5.0E-1	475.9	0.51	60,741
1393	Air	–	–	–	–	–	5.0E-1	5.0E-1	464.7	0.41	127,386
1395	Air	–	–	–	–	–	5.0E-1	5.0E-1	456.7	0.35	183,979
1397	Air	–	–	–	–	–	5.0E-1	5.0E-1	446.0	0.30	347,991
1398	Air	–	–	–	–	–	5.0E-1	5.0E-1	436.7	0.27	666,000
1399	Air	–	–	–	–	–	5.0E-1	5.0E-1	431.8	0.25	>1,900,000
1400	Air	–	–	–	–	–	5.0E-1	5.0E-1	427.4	0.25	1,775,000
288°C											
1408	Air	–	–	–	–	–	5.0E-1	5.0E-1	416.6	0.76	21,548
1790	Air	–	–	–	–	–	5.0E-3	5.0E-1	452.8	0.75	16,765
1409	Air	–	–	–	–	–	5.0E-1	5.0E-1	377.2	0.50	53,144
1410	Air	–	–	–	–	–	5.0E-1	5.0E-1	377.6	0.50	51,194
1792	Air						5.0E-3	5.0E-1	413.4	0.51	35,710
1407	Air	–	–	–	–	–	5.0E-1	5.0E-1	364.4	0.40	82,691
1430	Air	–	–	–	–	–	5.0E-1	5.0E-1	348.3	0.30	168,852
1435	Air	–	–	–	–	–	5.0E-1	5.0E-1	342.0	0.25	314,352
1480	Air	–	–	–	–	–	4.9E-1	4.9E-1	340.1	0.25	319,308
1485	Air	–	–	–	–	–	5.1E-1	5.1E-1	340.4	0.25	369,206
320°C											
1405	Air	–	–	–	–	–	5.0E-1	5.0E-1	426.0	0.75	20,425
1404	Air	–	–	–	–	–	5.0E-1	5.0E-1	387.4	0.50	47,011
1406	Air	–	–	–	–	–	5.0E-1	5.0E-1	371.6	0.40	82,691
288°C											
1796	PWR	5	6.4	20.20	–677	–673	5.0E-1	5.0E-1	403.6	0.80	12,500
1812	PWR	2	6.5	20.00	–689	–686	5.0E-2	5.0E-1	413.9	0.80	6,375
1791	PWR	4	6.5	19.23	–697	–697	5.0E-3	5.0E-1	441.9	0.77	3,040
1793	PWR	4	6.4	19.23	–699	–700	5.0E-3	5.0E-1	434.3	0.80	3,020
1794	PWR	4	6.4	20.00	–690	–689	5.0E-3	5.0E-1	390.9	0.50	7,370
1814	PWR	1	6.5	20.00	–694	–691	5.0E-2	5.0E-1	348.7	0.29	33,200
1426	Hi DO	>200	–	–	–	–	8.0E-1	8.0E-1	405.1	0.80	12,069
1427	Hi DO	>200	–	–	–	–	8.2E-2	8.2E-2	421.7	0.82	6,679
1428	Hi DO	>200	–	–	–	–	7.4E-3	7.4E-3	441.4	0.74	5,897
1797	Hi DO	750	5.9	0.076	199	64	5.0E-3	5.0E-1	437.3	0.78	4,520
1414	Hi DO	>200	–	–	–	–	5.0E-1	5.0E-1	375.3	0.50	26,230
1418	Hi DO	>200	–	–	–	–	5.0E-1	5.0E-1	375.5	0.50	25,714
1423	Hi DO	>200	–	–	–	–	5.0E-2	5.0E-2	378.8	0.50	17,812
1425	Hi DO	>200	–	–	–	–	4.9E-3	4.9E-3	393.2	0.49	13,684
1431	Hi DO	>200	–	–	–	–	2.9E-1	2.9E-1	356.5	0.29	116,754
1434	Hi DO	>200	–	–	–	–	2.9E-2	2.9E-2	350.0	0.29	40,643
1436	Hi DO	>200	–	–	–	–	2.5E-2	2.5E-2	354.0	0.25	>1,719,851
1512	Hi DO	>200	–	–	–	–	2.4E-1	2.4E-1	361.2	0.24	2,633,954

[a]PWR = simulated PWR water containing 2 ppm lithium and 1000 ppm boron.
[b]DO and ECPs measured in effluent.
[c]Conductivity of water measured in feedwater supply tank.

Table 3. Fatigue test results for Type 304 austenitic SS at 288°C

Test No.	Env.[a]	DO[b] (ppb)	pH at RT	Conductivity [c] (µS/cm)	ECP Pt mV (SHE)	ECP Steel mV (SHE)	Ten. Rate (%/s)	Comp. Rate (%/s)	Stress Range (MPa)	Strain Range (%)	Life N_{25} (Cycles)
1801	Air	–	–	–	–	–	4.0E-1	4.0E-1	419.2	0.76	24,500
1805	Air	–	–	–	–	–	4.0E-3	4.0E-1	467.9	0.76	14,410
1804	Air	–	–	–	–	–	4.0E-1	4.0E-1	382.8	0.51	61,680
1817	Air	–	–	–	–	–	4.0E-3	4.0E-1	421.7	0.51	42,180
1825	Air	–	–	–	–	–	4.0E-2	4.0E-1	394.4	0.30	>625,860
1846	Air	–	–	–	–	–	4.0E-2	4.0E-1	396.4	0.32	>316,000
1806	PWR	4	6.0	18.87	–678	–675	4.0E-1	4.0E-1	428.9	0.73	11,500
1810	PWR	5	6.4	18.89	–684	–681	4.0E-2	4.0E-1	447.6	0.77	5,800
1808	PWR	4	6.4	18.87	–689	–686	4.0E-3	4.0E-1	468.3	0.77	2,850
1821	PWR	2	6.5	22.22	–696	–693	4.0E-3	4.0E-1	474.3	0.76	2,420
1829	PWR	2	6.5	18.18	–701	–701	4.0E-4	4.0E-1	493.6	0.73	1,560
1834	PWR	2	6.5	18.18	–707	–708	9.0E-5	4.0E-1	535.9	0.69	1,415
1807	PWR	4	6.5	18.87	–681	–678	4.0E-1	4.0E-1	374.6	0.51	25,900
1823	PWR	3	6.6	23.06	–697	–695	4.0E-3	4.0E-1	408.2	0.51	6,900
1826	PWR	2	6.5	18.76	–707	–706	1.0E-2	4.0E-1	375.8	0.29	>89,860
1847	PWR	5	6.5	18.87	–696	–692	1.0E-2	4.0E-1	388.9	0.32	>165,300
1852	Hi DO	790	6.1	0.061	239	153	4.0E-1	4.0E-1	429.1	0.74	10,800
1827	Hi DO	850	6.0	0.086	258	80	4.0E-3	4.0E-1	475.8	0.75	3,650
1845	Hi DO	870	6.0	0.063	274	185	4.0E-4	4.0E-1	488.7	0.71	>7,310

[a]PWR = simulated PWR water containing 2 ppm lithium and 1000 ppm boron.
[b]DO and ECPs measured in effluent.
[c]Conductivity of water measured in feedwater supply tank.

Table 4. Fatigue test results for CF–8M cast SSs at 288°C

Test No.	Env.[a]	DO[b] (ppb)	pH at RT	Conductivity [c] (µS/cm)	ECP Pt mV (SHE)	ECP Steel mV (SHE)	Ten. Rate (%/s)	Comp. Rate (%/s)	Stress Range (MPa)	Strain Range (%)	Life N_{25} (Cycles)
1831	Air	–	–	–	–	–	4.0E-1	4.0E-1	429.7	0.76	26,500
1832	Air	–	–	–	–	–	4.0E-3	4.0E-1	534.0	0.76	9,050
1848	Air	–	–	–	–	–	4.0E-1	4.0E-1	440.7	0.76	17,900
1850	PWR	5	6.5	17.241	–691	–689	4.0E-3	4.0E-1	419.5	0.76	10,700
1854	PWR	2	6.5	18.692	–695	–691	4.0E-2	4.0E-1	448.4	0.75	4,720
1839	Air	–	–	–	–	–	4.0E-1	4.0E-1	474.2	0.76	15,290
1840	Air	–	–	–	–	–	4.0E-3	4.0E-1	534.8	0.75	19,800
1851	PWR	4	6.5	18.182	–696	–695	4.0E-1	4.0E-1	482.1	0.75	6,420
1844	PWR	2	6.5	18.182	–667	–680	4.0E-3	4.0E-1	527.7	0.72	2,180
1842	Hi DO	820	6.1	0.063	271	145	4.0E-3	4.0E-1	508.5	0.75	1,375
1835	Air	–	–	–	–	–	4.0E-3	4.0E-1	631.2	0.76	7,200
1843	PWR	2	6.5	18.182	–568	–576	4.0E-3	4.0E-1	625.3	0.80	1,464
1838	Hi DO	870	6.5	0.061	261	113	4.0E-3	4.0E-1	636.1	0.78	1,320

[a]PWR = simulated PWR water that contained 2 ppm lithium and 1000 ppm boron.
[b]DO and ECPs measured in effluent.
[c]Conductivity of water measured in feedwater supply tank.

3 Overview of Fatigue S–N Data

The relevant fatigue S–N data for austenitic SSs in air include the data compiled by Jaske and O'Donnell[36] for developing fatigue design criteria for pressure vessel alloys, the JNUFAD* data base from Japan, and the results of Conway et al.[37] and Keller.[38] In water, the existing fatigue S–N data include the tests performed by General Electric Co. (GE) in a test loop at the Dresden 1 reactor,[39] the JNUFAD data base, studies at Mitshubishi Heavy Industries, Ltd., (MHI),[21–24] Ishikawajima–Harima Heavy Industries Co., (IHI),[25] and Hitachi[26,27] in Japan, and the present work at ANL.[28–31] The data base for austenitic SSs is composed of 500 tests in air (240 tests on 26 heats of Type 304 SS, 170 tests on 15 heats of Type 316 SS, and 90 tests on 4 heats of Type 316 NG) and 290 tests in water (135 tests on 9 heats of Type 304 SS, 55 tests on 3 heats of Type 316 SS, and 100 tests on 4 heats of Type 316NG). Nearly 60% of the tests in air were conducted at room temperature, 20% at 250–325°C, and 20% at 350–450°C. Nearly 90% of the tests in water were conducted at temperatures between 260 and 325°C; the remainder were at lower temperatures. The data on Type 316NG in water have been obtained primarily at DO levels ≥0.2 ppm and those on Type 316 SS, at ≤0.005 ppm DO; half of the tests on Type 304 SS are at low–DO and the remaining at high–DO levels.

3.1 Air Environment

The existing fatigue S–N data, both domestic and from abroad, indicate that the fatigue lives of Types 304 and 316 SS are comparable; those of Type 316NG are superior. Fatigue life in air is independent of temperature in the range from room temperature to 427°C (Fig. 5). The three curves in Fig. 5 are based on the current ASME mean curve, the best–fit curve developed by Jaske and O'Donnell,[36] and the updated statistical model that is discussed later in this report. The results indicate that the ASME mean curve is not consistent with the existing fatigue S–N data for austenitic SSs. At strain amplitudes <0.5%, the mean curve predicts significantly longer fatigue lives than those observed experimentally. The results also indicate that at temperatures above 260°C, the fatigue life of austenitic SSs may decrease with decreasing strain rate (Fig. 6). The effect of strain rate on fatigue life seems to be significant at 400–430°C. However, other studies[40] have shown no effect of strain rate on the fatigue life of Type 316 SS at 0.4–0.008%/s strain rates and temperatures up to 450°C.

During cyclic loading, austenitic SSs exhibit rapid hardening during the first 50–100 cycles; the extent of hardening increases with increasing strain amplitude and decreasing temperature and strain rate.[27,28,41] The cyclic strain hardening of Type 316NG SS tested in air at room temperature and 288°C is shown in Fig. 7. The initial hardening is followed by softening and a saturation stage at 288°C, and by continuous softening at room temperature.

The cyclic stress–vs.–strain curves for Types 304, 316, and 316NG SS at room temperature and 288°C are shown in Fig. 8; cyclic stress corresponds to the value at half life and at a strain rate of 0.4%/s. For the various steels, cyclic stresses increase in magnitude in the following order: Types 316NG, 304, and 316. At room temperature, the strain amplitude ε_a(%) for Type 316 SS can be expressed in terms of the cyclic stress amplitude σ_a(MPa) by the equation

---

* M. Higuchi, Ishikawajima–Harima Heavy Industries Co., Japan, private communication to M. Prager of the Pressure Vessel Research Council, 1992.

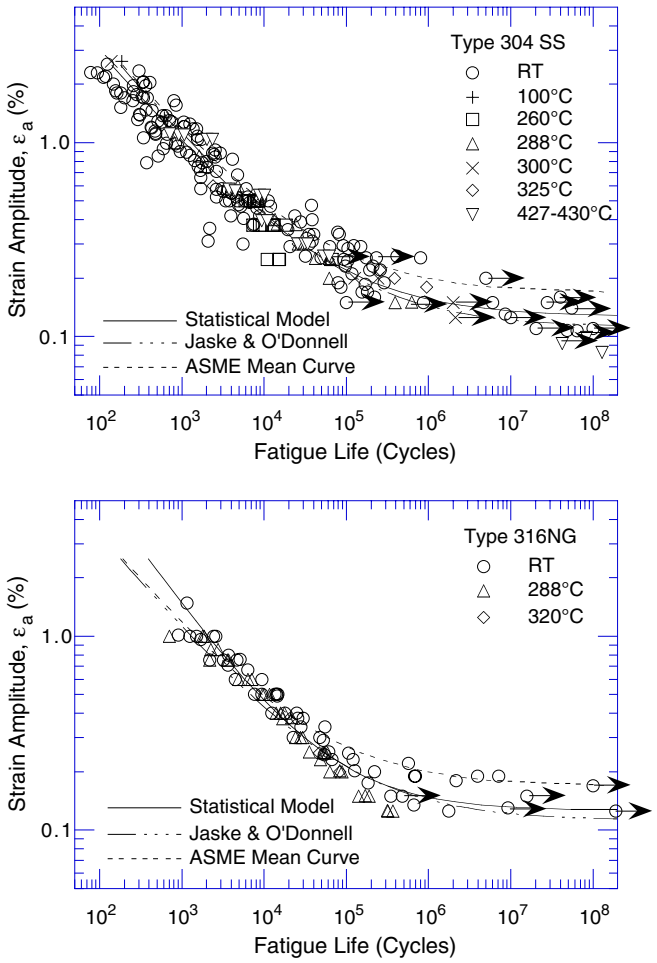

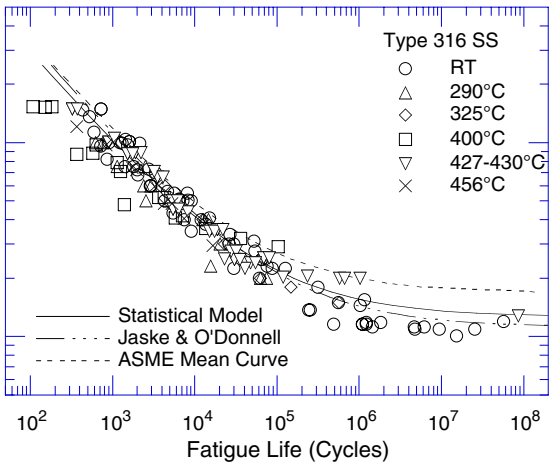

Figure 5.
Fatigue S–N behavior for Types 304, 316, and 316NG austenitic SSs in air at various temperatures

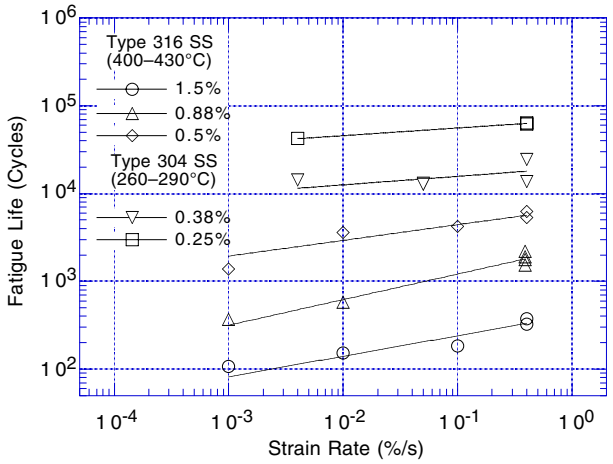

Figure 6.
Effect of strain rate on fatigue lives of austenitic SSs in air for various strain ranges

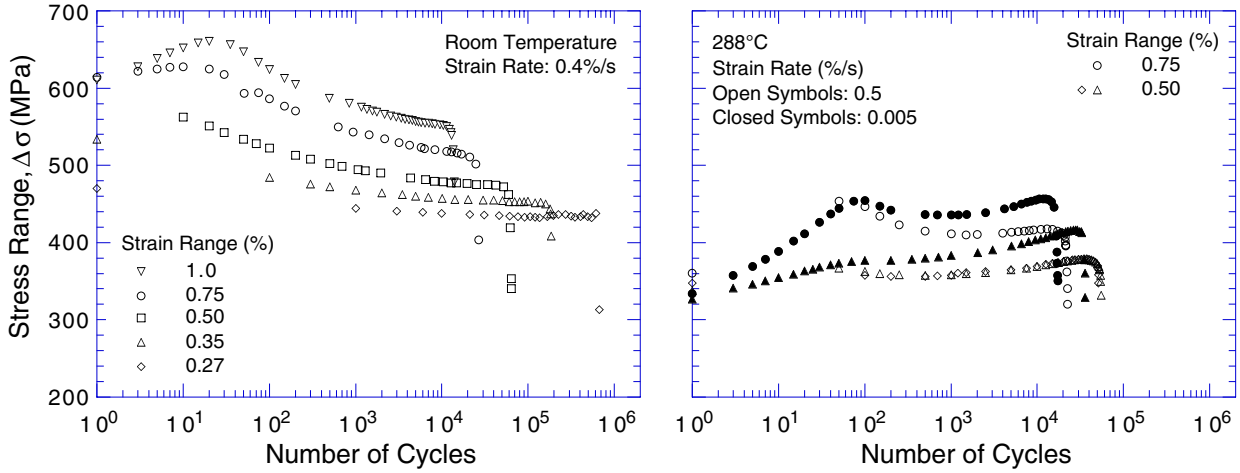

Figure 7. Effect of strain range on cyclic strain–hardening behavior of Type 316NG SS in air at room temperature and 288°C

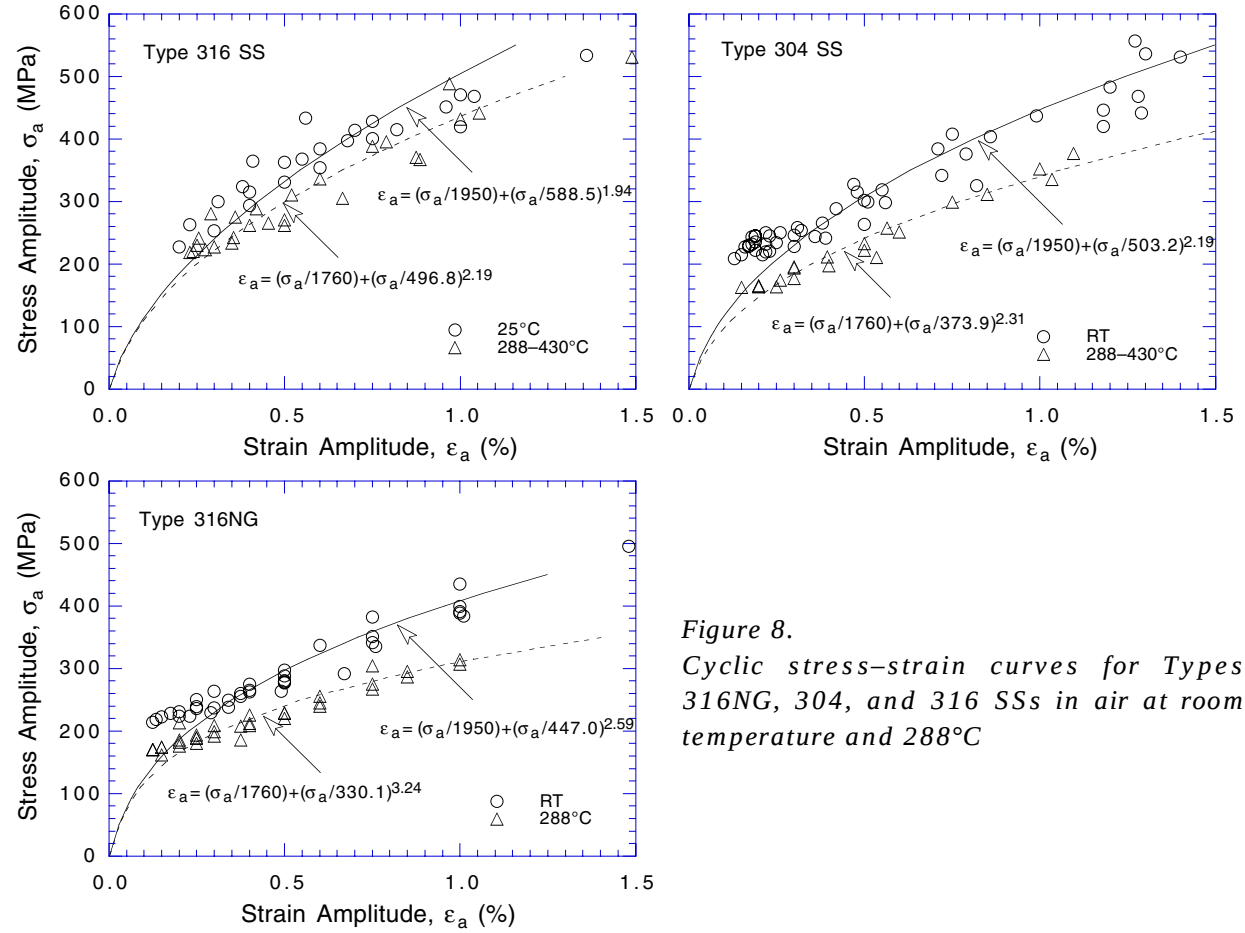

Figure 8. Cyclic stress–strain curves for Types 316NG, 304, and 316 SSs in air at room temperature and 288°C

$$\varepsilon_a = \frac{\sigma_a}{1950} + \left(\frac{\sigma_a}{588.5}\right)^{1.94}, \qquad (4a)$$

for Type 304 SS, by

$$\varepsilon_a = \frac{\sigma_a}{1950} + \left(\frac{\sigma_a}{503.2}\right)^{2.19}, \tag{4b}$$

and for Type 316NG, by

$$\varepsilon_a = \frac{\sigma_a}{1950} + \left(\frac{\sigma_a}{447.0}\right)^{2.59}. \tag{4c}$$

At 288–430°C, the cyclic stress–vs.–strain curve for Type 316 SS can be expressed by

$$\varepsilon_a = \frac{\sigma_a}{1760} + \left(\frac{\sigma_a}{496.8}\right)^{2.19}, \tag{4d}$$

for Type 304 SS, by

$$\varepsilon_a = \frac{\sigma_a}{1760} + \left(\frac{\sigma_a}{373.9}\right)^{2.31}, \tag{4e}$$

and for Type 316NG, by

$$\varepsilon_a = \frac{\sigma_a}{1760} + \left(\frac{\sigma_a}{330.1}\right)^{3.24}. \tag{4f}$$

3.2 LWR Environments

The fatigue S–N data indicate a significant decrease in fatigue life in LWR environments (Fig. 9). The reduction in life depends on strain rate, DO level in water, and temperature.[21–31] Also, environmental effects on fatigue life are comparable for all steels. To define the threshold values, the effects of various parameters on fatigue life are discussed below in greater detail.

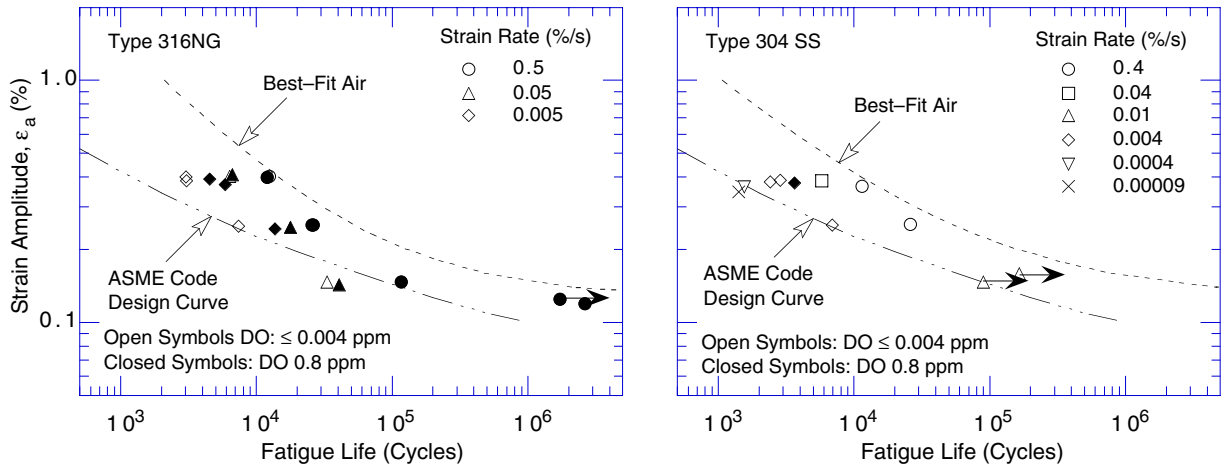

Figure 9. Fatigue strain amplitude–vs.–life data for Types 316NG and 304 SS in water at 288°C

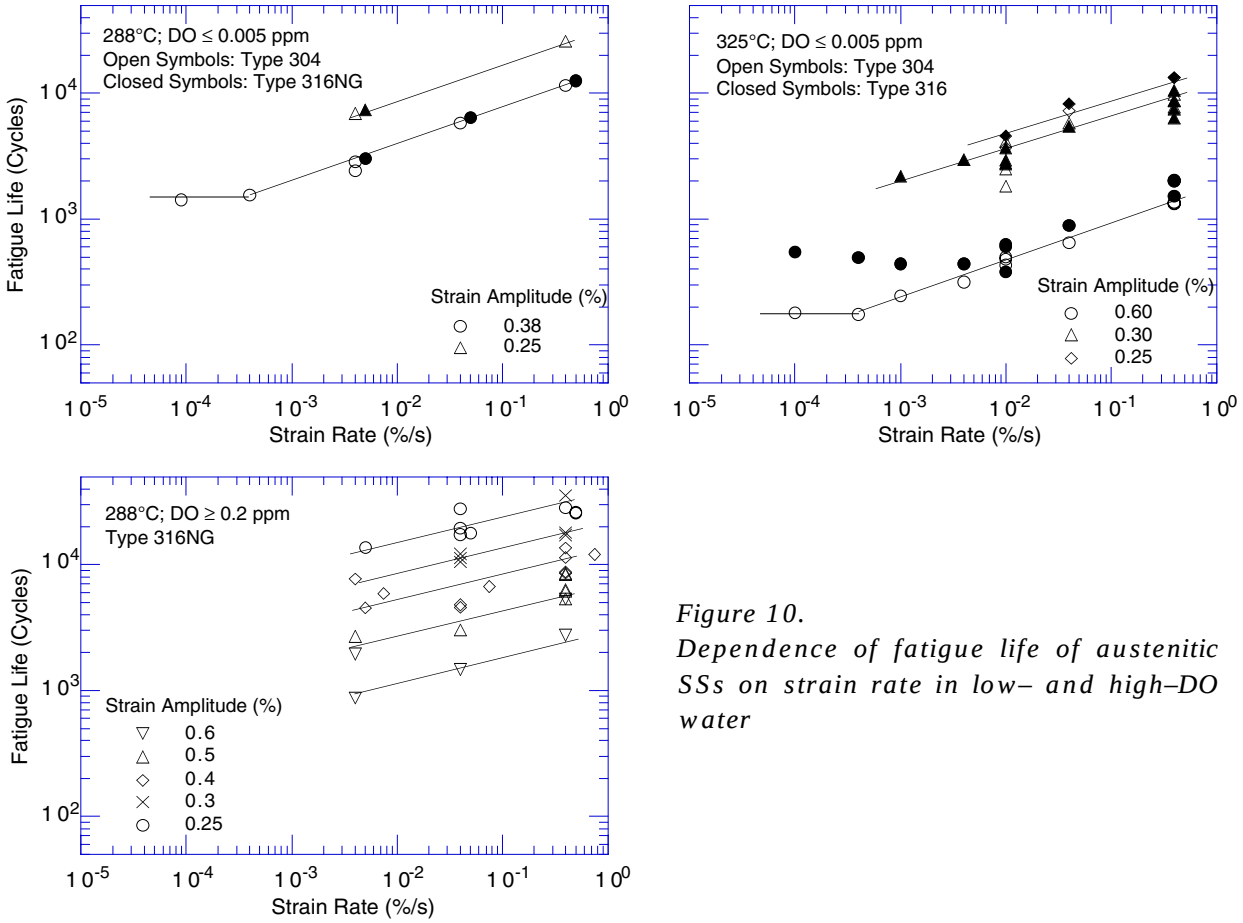

Figure 10. Dependence of fatigue life of austenitic SSs on strain rate in low– and high–DO water

3.2.1 Strain Rate

A slow strain rate applied during the tensile–loading cycle (i.e., up–ramp with increasing strain) is primarily responsible for environmentally assisted reduction in fatigue life. Slow rates applied during both tensile– and compressive–loading cycles (i.e., up– and down–ramps) do not cause further decrease in fatigue life.[29–31] The fatigue lives of austenitic SSs in low– and high–DO water are plotted as a function of tensile strain rate in Fig. 10. At both low– and high–DO levels, fatigue lives decrease with decreasing strain rate. The effect of strain rate is greater in a low–DO PWR environment than in high–DO water. In a simulated PWR environment, a decrease in strain rate from 0.4 to 0.0004%/s decreases fatigue life by a factor of ≈10. The results indicate that the strain rate below which effects of strain rate on fatigue life saturate may depend on both steel type and DO level. In low–DO PWR environments, saturation strain rate appears to be at ≈0.0004%/s for Type 304 SS and somewhat higher for Type 316 SS (best estimate of ≈0.004%/s). Limited data suggest that the saturation strain rate is also higher in high– than in low–DO water.

3.2.2 Strain Amplitude

Nearly all of the existing fatigue S–N data have been obtained under loading histories with constant strain rate, temperature, and strain amplitude. Actual loading histories encountered

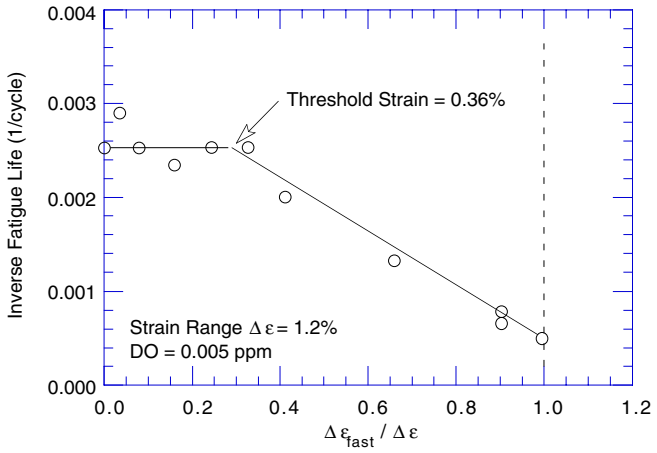

Figure 11.
Results of strain rate change tests on Type 316 SS in low–DO water at 325°C

during service of nuclear power plants are far more complex. Exploratory fatigue tests have been conducted with waveforms in which the slow strain rate is applied during only a fraction of the tensile loading cycle.[24] The results indicate that a minimum threshold strain is required to produce an environmentally assisted decrease in fatigue life of these steels. Figure 11 shows that, for a heat of Type 316 SS, the threshold strain in low–DO water at 325°C is ≈0.36%. During each cycle, relative damage due to slow strain rate is the same once the strain amplitude exceeds the threshold value.

Fatigue data from the present study indicate a threshold strain range of ≈0.32% for the ANL heat of Type 304 SS. For example, the test at 0.15% strain amplitude and 0.01%/s strain rate (as shown by a runoff triangle symbol in Fig. 9), failed after an additional 41,240 cycles when the strain amplitude was increased to 0.16%. Another test at 0.16% strain amplitude failed after an additional 50,700 cycles at 0.17% strain amplitude. The threshold strain most likely corresponds to rupture strain of the passive oxide film. These results are similar to those observed for carbon and low–alloy steels.[16–20]

3.2.3 Dissolved Oxygen

The results also indicate that environmental effects on the fatigue life of austenitic SSs differ from those on carbon and low–alloy steels; they are more pronounced in low–DO than in high–DO water.[18,19] At a strain rate of 0.004%/s, the reduction in fatigue life of Type 316NG (Fig. 10) is greater by a factor of ≈2 in a simulated PWR environment (<0.01 ppm DO) than in high–DO water (≥0.2 ppm DO). For carbon and low–alloy steels, environmental effects on fatigue life increase with increasing DO content above a minimum threshold value of 0.05 ppm; only a modest decrease in life is observed at DO levels <0.05 ppm.[11–13,16–20]

Existing data are inadequate to establish the functional form for the dependence of fatigue life of austenitic SSs on DO level. Recent test results indicate that the fatigue lives of austenitic SSs may depend on the conductivity of the water rather than on the DO content, e.g., fatigue life is longer at lower conductivity (<0.1 μS/cm). In the existing fatigue S–N data base, most of the tests in high–DO water have been performed at conductivities up to 0.2 μS/cm. Recent tests in high–DO water with conductivities <0.08 μS/cm show only a modest effect of environment on the fatigue lives of these steels. Tests are in progress to establish the effects of water chemistry on the fatigue lives of austenitic SSs.

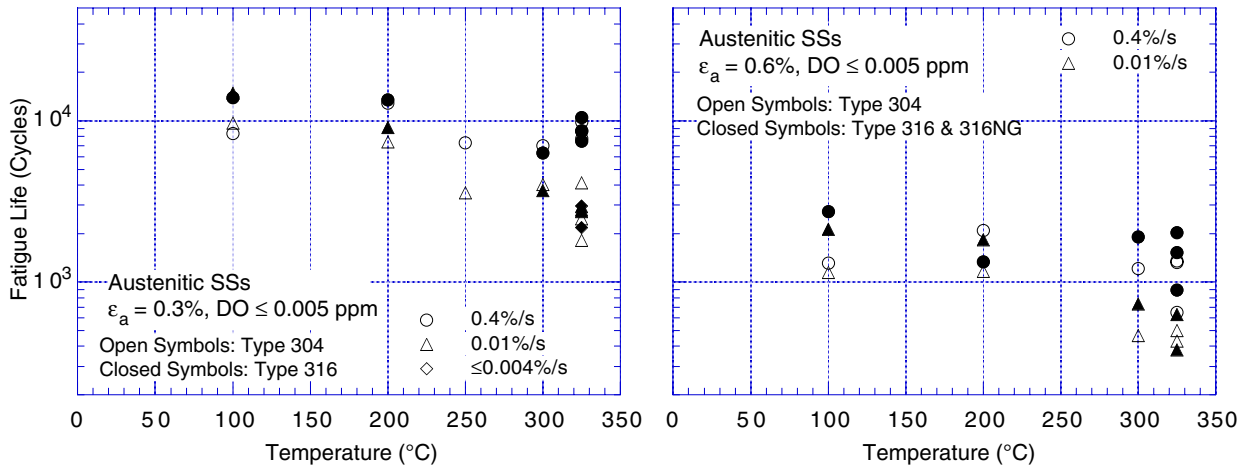

Figure 12. Change in fatigue lives of austenitic SSs in low–DO water with temperature

3.2.4 Temperature

The existing fatigue S–N data are inadequate to establish the functional form for the dependence of life on temperature. Limited data indicate that environmental effects on the fatigue lives of austenitic SSs are significant at temperatures above 250°C and are minimal at temperatures ≤200°C (Fig. 12). At 250–330°C, fatigue life appears to be relatively insensitive to changes in temperature.

As discussed in the previous section, actual loading histories encountered during service in nuclear power plants involve variable loading and environmental conditions, whereas the existing fatigue S–N data have been obtained under loading histories with constant strain rate, temperature, and strain amplitude. Fatigue tests have been conducted at MHI Japan on Type 316 SS under combined mechanical and thermal cycling.[24] Triangular waveforms were used for both strain and temperature cycling. Two sequences were selected for temperature cycling (Fig. 13): an in–phase sequence, in which temperature cycling was synchronized with mechanical strain cycling; and a sequence in which temperature and strain were out of phase, i.e., maximum temperature occurred at minimum strain level and vice-versa. Two temperature ranges, 100–325°C and 200–325°C, were selected for the tests.

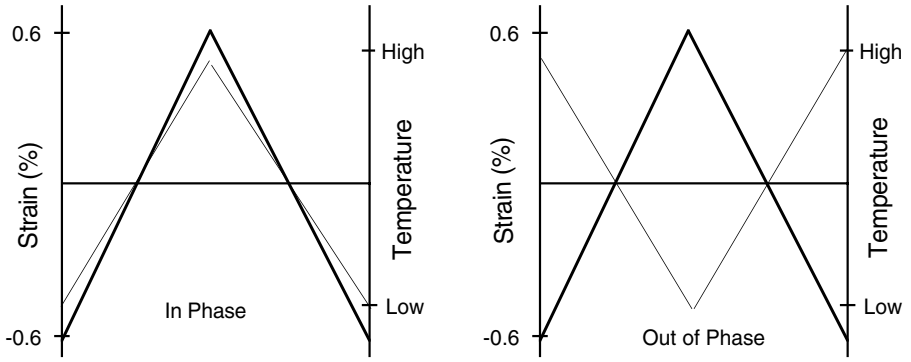

Figure 13. Waveforms for change in temperature during exploratory fatigue tests

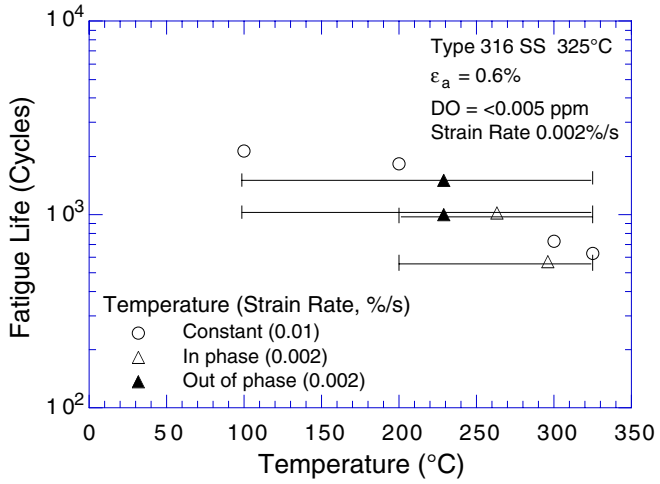

Figure 14.
Fatigue life of Type 316 SS under varying temperature, indicated by horizontal bars

The results are shown in Fig. 14, with the data obtained from tests at constant temperature. If we consider that the tensile–load cycle is primarily responsible for environmentally assisted reduction in fatigue life and that the applied strain and temperature must be above a minimum threshold value for environmental effects to occur, then, life should be longer for out–of–phase tests than for in–phase tests, because applied strains above the threshold strain occur at temperatures above 200°C for in–phase tests, whereas they occur at temperatures below 200°C for out–of–phase tests. An average temperature is used in Fig. 14 for the thermal cycling tests, i.e., the average of the temperature at peak strain and the temperature at threshold strain or 200°C (whichever is higher). The results from thermal cycling tests agree well with those from constant–temperature tests. The data suggest a linear decrease in life at temperatures above 200°C. Fatigue tests are in progress at 200–320°C to establish the temperature dependence of fatigue life in LWR environments.

3.3 Cast Stainless Steels

Available fatigue S–N data[23,31] indicate that in air, the fatigue lives of cast CF–8 and CF–8M SSs are similar to that of wrought austenitic SSs (Fig. 15). It is well known that the Charpy impact and fracture toughness properties of cast SSs are decreased significantly after thermal aging at temperatures between 300 and 450°C.[42,43] The cyclic–hardening behavior of cast SSs is also influenced by thermal aging (Fig. 16). At 288°C, cyclic stresses of steels aged for 10,000 h at 400°C are higher than those for unaged material or wrought SSs. Also, strain rate effects on cyclic stress are greater for aged than for unaged steel, i.e., cyclic stresses increase significantly with decreasing strain rate. However, existing data are inadequate to establish unequivocally the effect of thermal aging on the fatigue life of these steels. For example, thermal aging for 25,200 h at 465°C exerted no effect on the fatigue life of a CF-8M steel in air at 325°C,[24] whereas, in the present study, aging for 10,000 h at 400°C decreased the fatigue life of Heat 74 at 288°C, particularly in water (discussed later in this section). These differences are most likely caused by microstructural differences that arise from thermal aging temperature. Aging at 400°C results in spinodal decomposition of the ferrite to form Cr–rich regions that very effectively increase tensile strength, whereas, aging at 465°C for extended periods results in the formation of Cr–rich α' particles and over–aging.

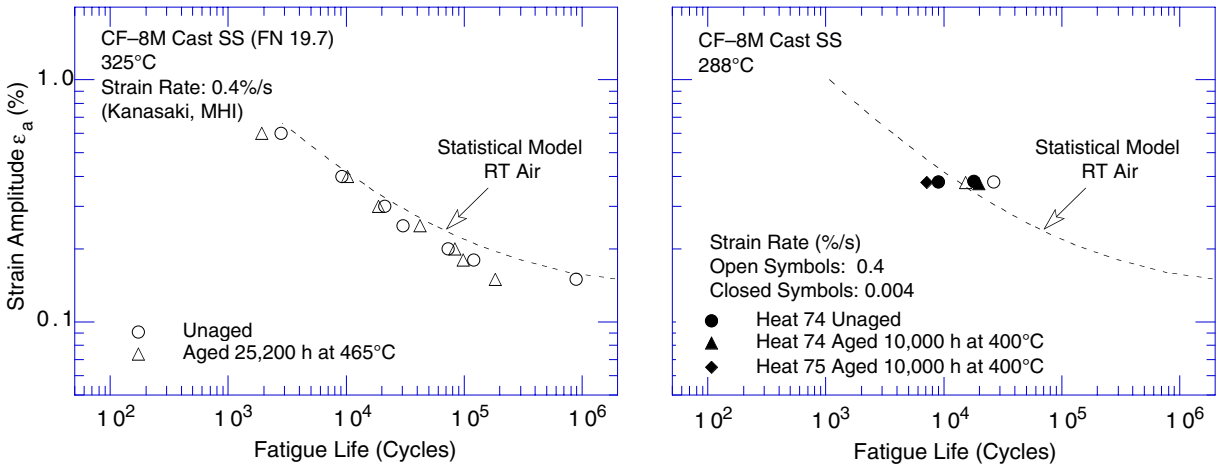

Figure 15. Fatigue strain amplitude–vs.–life data for CF–8M cast SSs in air

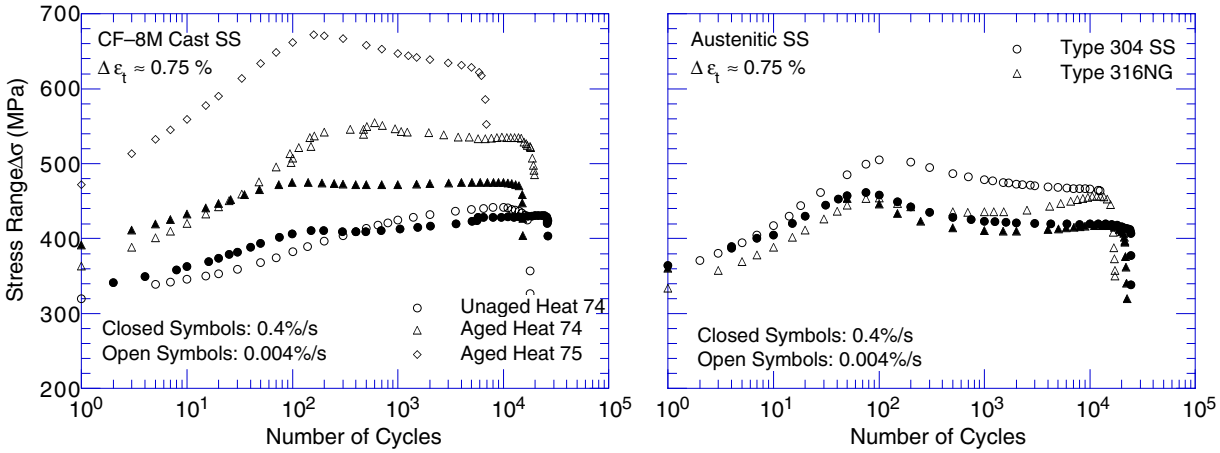

Figure 16. Effect of strain rate on cyclic–hardening behavior of wrought and cast SSs in air at 288°C

The existing fatigue S–N data[23,31] for cast SSs in LWR environments indicate that the fatigue lives of cast SSs are approximately the same in both high– or low–DO water and are comparable to those observed for wrought SSs in low–DO water (Fig. 17). The results also indicate that thermal aging decreases the fatigue lives of these steels. The reduction in life in LWR environments depends on strain rate (Fig. 18). The effects of strain rate are the same in low– and high–DO water. Existing data are inadequate to establish the saturation strain rate for cast SSs. For unaged material, environmental effects on life do not appear to saturate at strain rates as low as 0.00001%/s.[23] Also, the fatigue lives of these steels are relatively insensitive to changes in ferrite content in the range of 12–28%.[23]

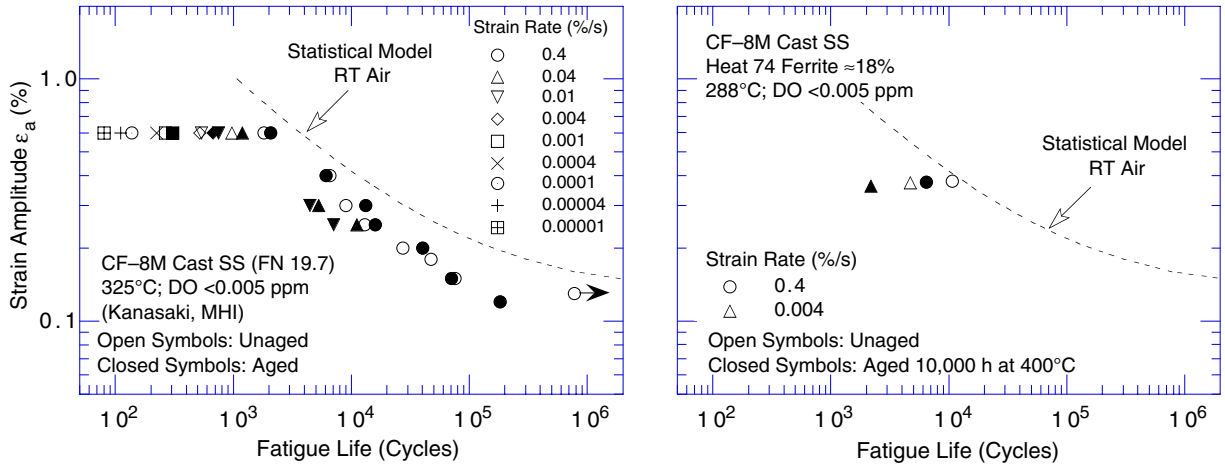

Figure 17. Fatigue strain amplitude–vs.–life data for CF–8M cast SSs in water

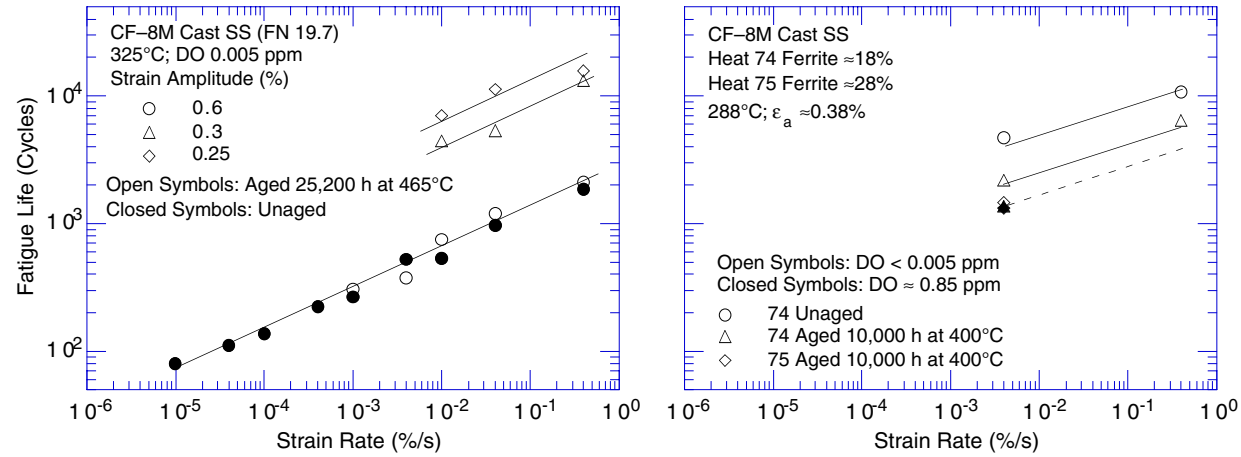

Figure 18. Dependence of fatigue lives of CF–8M cast SSs on strain rate in low–DO water at various strain amplitudes

4 Mechanism of Fatigue Crack Initiation

4.1 Formation of Engineering Cracks

The formation of surface cracks and their growth to an "engineering" size (3 mm deep) constitute the fatigue life of a material, which is represented by the fatigue S–N curves. Fatigue life has conventionally been divided into two stages: initiation, expressed as the cycles required to form microcracks on the surface; and propagation, expressed as cycles required to propagate the surface cracks to engineering size. During cyclic straining, microcracks form at surface irregularities / discontinuities either already in existence or produced by slip bands, grain boundaries, second–phase particles, etc. Once a microcrack forms, it continues to grow along its slip plane as a Mode II (shear) crack in Stage I growth (orientation of the crack is usually at 45° to the stress axis). At low strain amplitudes, a Stage I crack may extend across several grain diameters before the increasing stress intensity of the crack promotes slip on systems other than the primary slip. A dislocation cell structure normally forms at the crack

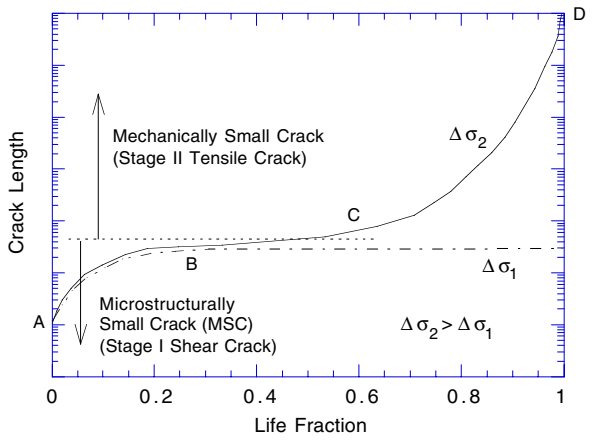

Figure 19.
Growth of cracks in smooth fatigue specimens

tip. Because slip is no longer confined to planes at 45° to the stress axis, the crack begins to propagate as a Mode I (tensile) crack, normal to the stress axis in Stage II growth. At high strain amplitudes, the stress intensity is quite large and the crack propagates entirely by the Stage II process. Stage II crack propagation continues until the crack reaches engineering size (≈3 mm deep). In air or mildly corrosive environments, Stage II cracking is characterized by fatigue striations.

An alternative approach considers fatigue life to be entirely composed of the growth of short surface cracks.[44] In polycrystalline materials, the period for the formation of surface cracks is negligible, Fig. 19. However, the growth rates of short cracks cannot be predicted accurately from fracture mechanics methodology on the basis of the range of the stress intensity factor (ΔK). Under cyclic loading and the same ΔK, short fatigue cracks (i.e., with lengths comparable to the unit size of the microstructure) grow at a faster rate than long fatigue cracks.[45] Also, short cracks can grow at ΔK values below those predicted from linear elastic fracture mechanics (LEFM). The differences between the growth rates of short and long cracks have been attributed to interactions among microstructural features, contributions of crack closure with increasing crack length, effects of mixed–mode crack propagation, and an inadequate characterization of the crack tip stress/strain fields associated with short cracks.

Recent studies indicate that during fatigue loading of smooth test specimens, surface cracks 10 μm or longer form quite early, i.e., <10% of life, even at low strain amplitudes.[46,47] Growth of these surface cracks may be divided into three regimes: (a) initial period that involves growth of microstructurally small cracks (MSCs) below a critical length, characterized by decelerating crack growth rate, seen in region AB of Fig. 19; (b) final period of growth, characterized by accelerating crack growth rate, region CD; and (c) a transition period controlled by a combination of the two regimes, region BC. The crack growth rates as a function of crack length during the three regimes of fatigue life are shown in Fig. 20.

The growth of MSCs is very sensitive to microstructure.[46,48] The MSCs correspond to Stage I cracks and grow along slip planes as shear cracks in the early stage of growth. Microstructural effects on MSCs are strong because of Stage I growth, i.e., crystallographic growth. Fatigue cracks greater than the critical length of MSCs show little or no influence of microstructure and are termed mechanically small cracks. For a stress ratio of –1, the transition from an MSC to a mechanically small crack for several materials has been estimated

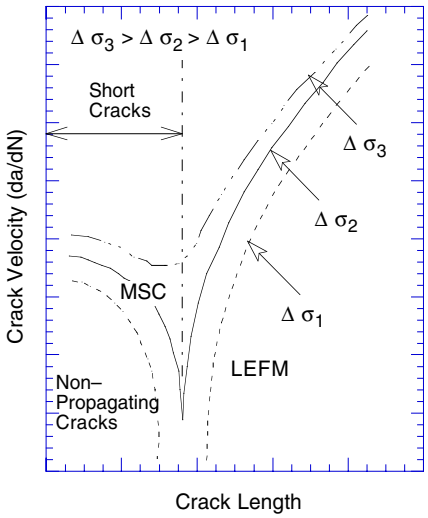

Figure 20.
Schematic illustration of short–crack behavior

to be ≈8 times the unit size of the microstructure.[48] Mechanically small cracks correspond to Stage II (tensile) cracks, which are characterized by striated crack growth, with a fracture surface normal to the maximum principal stress.

At low stress levels, e.g., $\Delta\sigma_1$ in Figs. 19 and 20, the transition from MSC growth to accelerating crack growth does not occur and the cracks are nonpropagating. This circumstance represents the fatigue limit for the smooth specimen. Although cracks can form below the fatigue limit, they can grow to engineering size only at stresses greater than the fatigue limit. Possible preexisting large cracks in the material, e.g., defects in welded samples, or those created by growth of microcracks at high stresses, can grow at stress levels below the fatigue limit, and their growth can be estimated from ΔK–based LEFM.

4.2 Environmental Effects

The reduction in fatigue life in LWR coolant environments may arise from easy formation of surface microcracks and/or an increase in growth rates of cracks during either the initial stage of MSC and shear crack growth or during the transition and final stage of tensile crack growth. Photomicrographs of the gauge surface of Type 316NG specimens tested in air, simulated PWR water, and high–DO water are shown in Fig. 21. Specimens tested in water contain crystalline oxides and a thin gray corrosion scale. X–ray diffraction analyses of specimens tested in water indicate that the corrosion scale consists primarily of magnetite (Fe_3O_4) or ferroferric oxide ($FeFe_2O_4$), chromium oxide (CrO), and maghemite (γ–Fe_2O_3). In addition to these phases, specimens tested in high–DO water also contained hematite (ferric oxide or α–Fe_2O_3). The specimens tested in water also show some surface micropitting.

The reduction in fatigue life in high–temperature water has often been attributed to the presence of micropits[10] that act as stress raisers and provide preferred sites for the formation of fatigue cracks. However, the fatigue data for carbon and low–alloy steel indicate that the large reductions in the fatigue lives of these steels in LWR environments cannot be explained on the basis of micropits alone.[18–20] If the presence of micropits was responsible for reducing the fatigue lives of carbon and low–alloy steels in LWR environments, specimens preexposed to high–DO water and then tested in air should also show a decrease in fatigue life. Fatigue lives

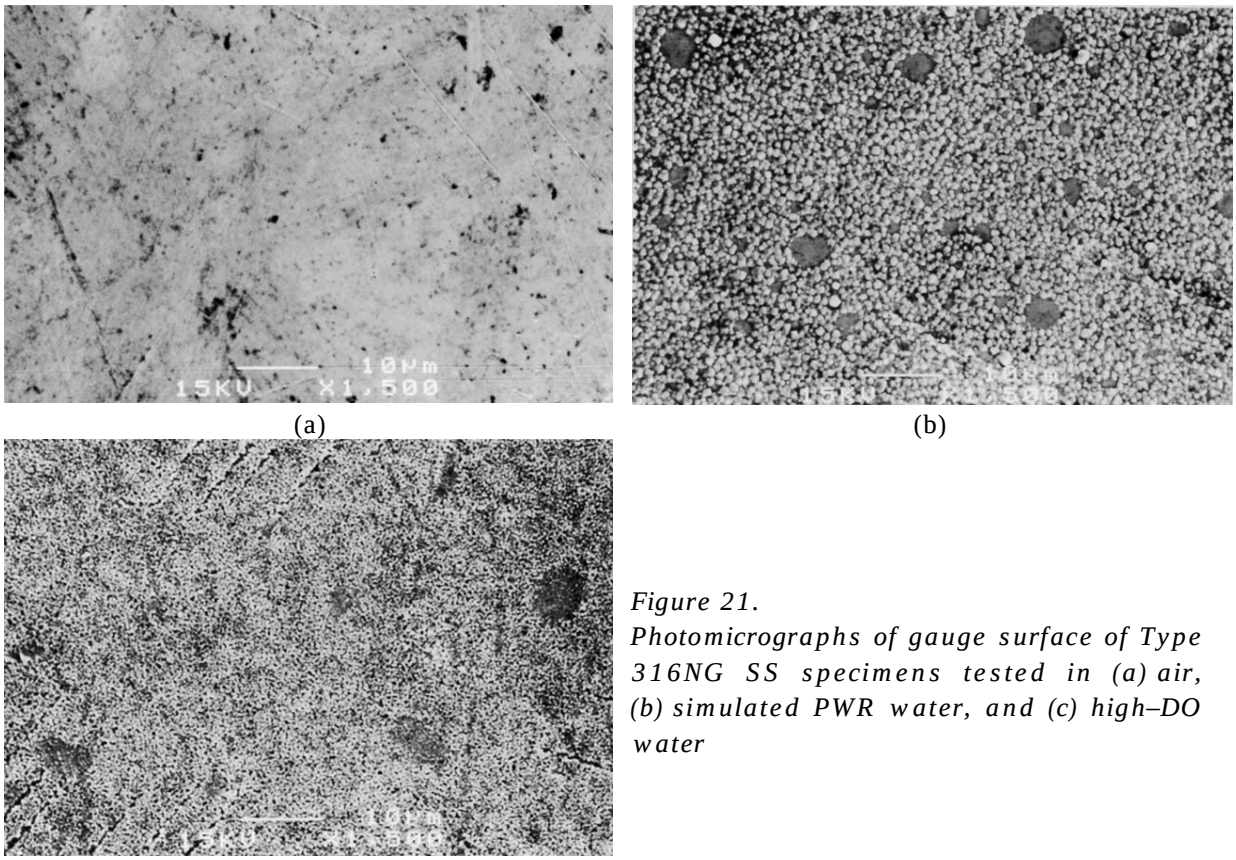

Figure 21.
Photomicrographs of gauge surface of Type 316NG SS specimens tested in (a) air, (b) simulated PWR water, and (c) high–DO water

of the preoxidized and unoxidized specimens are identical; life would be expected to decrease if surface micropits facilitate the formation of fatigue cracks.[18–20] Only a moderate decrease in life is observed for both preoxidized and unoxidized specimens that were tested in low–DO water. The significant reduction in fatigue life in LWR coolant environments may be attributed to enhanced growth rates of cracks either during the initial growth stage of microstructurally small and shear cracks or the transition and final stage of tensile crack growth.

The enhanced growth rates of long cracks in pressure vessel and piping steels in LWR environments have been attributed to either slip oxidation/dissolution[49] or hydrogen–induced cracking[50] mechanisms. The requirements for a slip dissolution model are that a protective oxide film is thermodynamically stable to ensure that a crack will propagate with a high aspect ratio without degrading into a blunt pit, and that a strain increment occurs to rupture that film and thereby expose the underlying matrix to the environment; see Fig. 22. Once the passive oxide film is ruptured, crack extension is controlled by dissolution of freshly exposed surfaces and by the oxidation characteristics.

Hydrogen–induced cracking is explained as follows: hydrogen produced by the oxidation reaction at or near the crack tip is partly absorbed into the metal; the absorbed hydrogen diffuses ahead of the crack tip, interacts with inclusions, and leads to the formation of cleavage cracks at the inclusion/matrix interface; and linkage of the cleavage cracks leads to discontinuous crack extension in addition to extension caused by mechanical fatigue. Other hydrogen–induced fracture processes may also enhance growth rates in LWR environments.

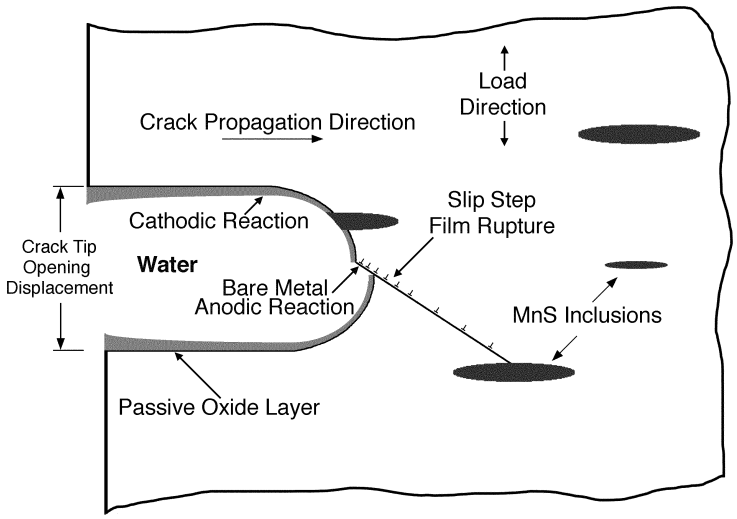

Figure 22.
Schematic illustration of film rupture/slip dissolution process

For example, significant accumulation of hydrogen at or near the crack tip decreases the cohesive interatomic strength of the lattice. Thus, hydrogen–induced bond rupture ahead of the crack tip links up with the main crack, producing discontinuous but enhanced crack growth. The hydrogen adsorption mechanism states that adsorbed hydrogen lowers the surface energy of the metal and thus facilitates crack growth at a lower fracture stress level. Also, hydrogen can cause localized crack tip plasticity by reducing the stress required for dislocation motion.

Both mechanisms depend on the rates of oxide rupture, passivation, and liquid diffusion. Therefore, it is often difficult to differentiate between the two processes or to establish their relative contribution to crack growth in LWR environments. Studies on crack initiation in smooth fatigue specimens indicate that the decrease in fatigue lives of carbon and low–alloy steels in LWR environments is caused primarily by the effects of environment on the growth of cracks that are <100 μm deep.[18–20,47] For cracks <100 μm deep, the growth rates are nearly two orders of magnitude higher in high–DO water than in air. For cracks >100 μm deep. the growth rates are one order of magnitude higher in high–DO water than in air. In LWR environments, crack initiation in carbon and low–alloy steels may be explained as follows: (a) surface microcracks form quite early in fatigue life; (b) during cyclic loading, the protective oxide film is ruptured at strains greater than the fracture strain of surface oxides, and the microcracks grow by anodic dissolution of the freshly exposed surface to crack depths greater than the critical length of MSCs; and (c) a final period of growth that can be predicted from fracture mechanics methodology and is characterized by accelerating growth rates.

For austenitic SSs, lower fatigue lives in low–DO water than in high–DO water are difficult to reconcile in terms of the slip oxidation/dissolution mechanism. In general, crack growth rates increase with increasing DO in the water. It may be argued that the lower lives in low–DO water are due to a lower rupture strain for surface oxides in low–DO than in high–DO water. As discussed above, oxide rupture strain in low–DO water may be in the range of 0.32–0.36%. The rupture strain in high–DO water must be significantly higher than this value to produce the observed difference of a factor of ≈2 in fatigue life. Metallographic examinations of the test specimens indicate that environmentally assisted reduction in fatigue lives of austenitic SSs is most likely caused by hydrogen–induced cracking.[29–31] Figure 23 shows photomicrographs of fracture surfaces of Type 304 and 316NG, after chemical cleaning and at

Type 304 SS Type 316NG SS

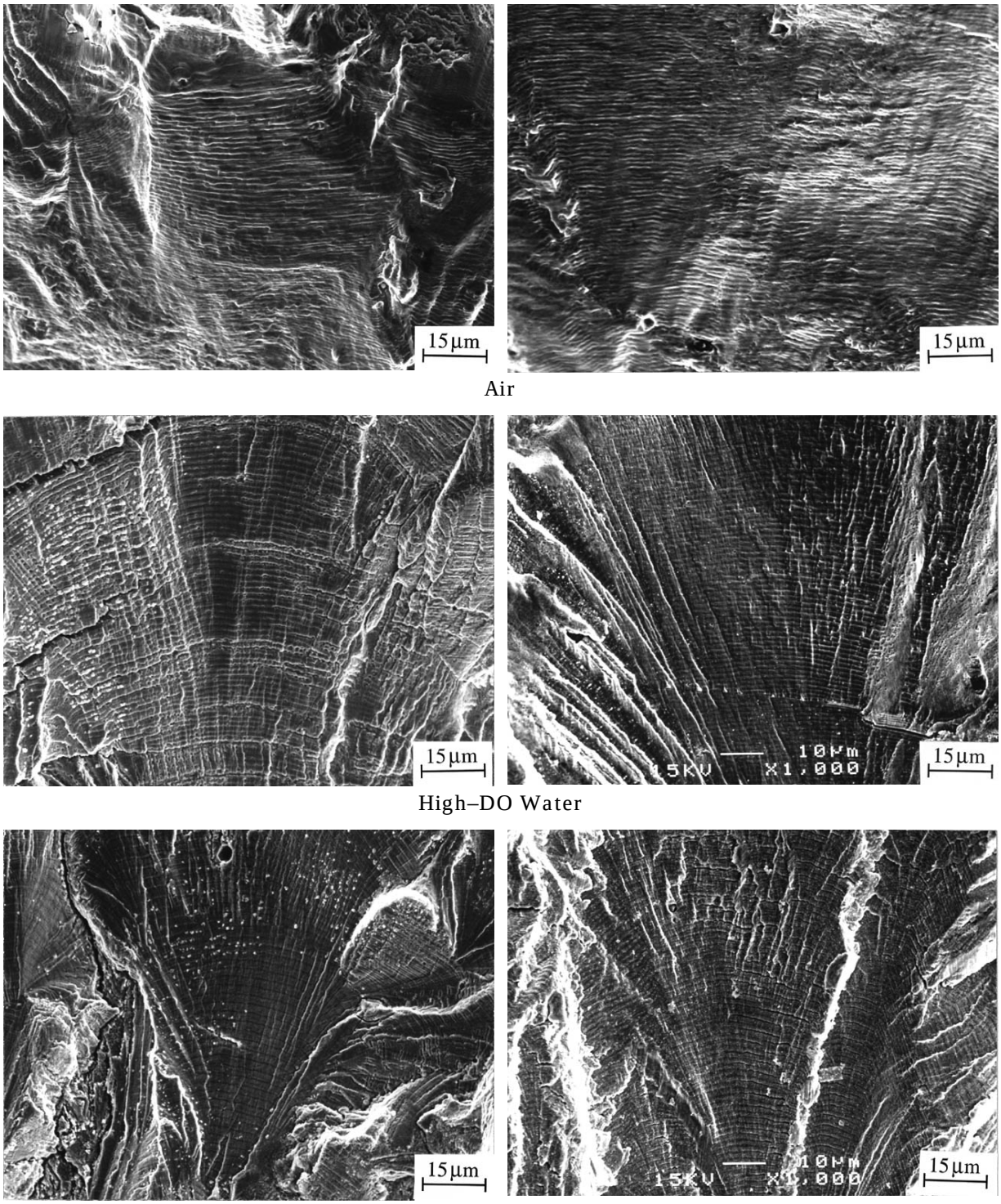

Figure 23. Photomicrographs of fracture surfaces of Types 304 and 316NG SS specimens tested in air, high–DO water, and low–DO, simulated PWR water

approximately the same crack length; specimens were tested at 288°C and ≈0.75% strain range in air, high–DO water, and a low–DO simulated PWR water. All of the specimens show fatigue striations; the spacing between striations indicates that crack growth increases in the following sequence: air, high–DO water, and low–DO PWR water. The presence of well defined striations suggests that the enhanced crack growth rates in austenitic SSs are most likely due to

hydrogen–induced cracking. Fatigue striations should not be observed if enhancement of crack growth is caused by the slip oxidation/dissolution process.

5 Statistical Model

The fatigue S–N curves are generally expressed in terms of the Langer equation,[6] which may be used to represent either strain amplitude in terms of life or life in terms of strain amplitude. The parameters of the equation are commonly established through least–squares curve–fitting of the data to minimize the sum of the square of the residual errors for either fatigue life or strain amplitude. A predictive model based on least–squares fit on life is biased for low strain amplitude. The model leads to probability curves that converge to a single value of strain, and fails to address the fact that at low strain values, most of the error in life is due to uncertainty associated with either measurement of strain or variation in fatigue limit caused by material variability. On the other hand, a least–squares fit on strain does not work well for higher strain amplitudes. Statistical models have been developed at ANL[33,34] by combining the two approaches and minimizing the sum of the squared Cartesian distances from the data point to the predicted curve; the models were later updated with a larger fatigue S–N data base.[31] The functional forms and transformation for the different variables were based on experimental observations and data trends.

In air, the model assumes that fatigue life is independent of temperature and that strain rate effects occur at temperatures >250°C. It is also assumed that the effect of strain rate on life depends on temperature. One data set, obtained on Type 316 SS in room–temperature air, was excluded from the analysis. The tests in this data set were conducted in load–control mode at stress levels in the range of 190–230 MPa. The strain amplitudes were calculated only as elastic strains, i.e., strain amplitudes of 0.1–0.12% (the data are shown as circles in Fig. 5, with fatigue lives of 4×10^5 to 3×10^7). Based on cyclic stress vs. strain correlations for Type 316 SS (Eqs. 4a–4f), actual strain amplitudes for these tests should be 0.23–0.32%. In air, the fatigue life N of Types 304 and 316 SS is expressed as

$$\ln(N) = 6.703 - 2.030 \ln(\varepsilon_a - 0.126) + T^* \dot{\varepsilon}^* \qquad (5a)$$

and that of Type 316NG, as

$$\ln(N) = 7.422 - 1.671 \ln(\varepsilon_a - 0.126) + T^* \dot{\varepsilon}^*, \qquad (5b)$$

where ε_a is the strain amplitude (%) and T^* and $\dot{\varepsilon}^*$ are transformed temperature and strain rate, respectively, defined as follows:

$$\begin{aligned} T^* &= 0 && (T < 250°C) \\ T^* &= [(T - 250)/525]^{0.84} && (250 \le T < 400°C) \end{aligned} \qquad (6a)$$

$$\begin{aligned} \dot{\varepsilon}^* &= 0 && (\dot{\varepsilon} > 0.4\%/s) \\ \dot{\varepsilon}^* &= \ln(\dot{\varepsilon}/0.4) && (0.0004 \le \dot{\varepsilon} \le 0.4\%/s) \\ \dot{\varepsilon}^* &= \ln(0.0004/0.4) && (\dot{\varepsilon} < 0.0004\%/s). \end{aligned} \qquad (6b)$$

In LWR environments, the fatigue lives of austenitic SSs depends on strain rate, DO level, and temperature; the decrease in life is greater at low–DO levels and high temperatures. However, existing data are inadequate to establish the functional form for the dependence of fatigue life on DO level or temperature. Separate correlations have been developed for low– and high–DO levels (< or ≥ 0.05 ppm), and low and high temperatures (< or ≥ 200°C). Also, a threshold strain rate of

0.4%/s and saturation rate of 0.0004%/s is assumed in the model. Furthermore, for convenience in incorporating environmental effects into fatigue evaluations, the slope of the S–N curve in LWR environments was assumed to be the same as that in air although the best–fit of the experimental data in water yielded a slope for the S–N curve that differed from the slope of the curve that was obtained in air. In LWR environments, the fatigue life N of Types 304 and 316 SS is expressed as

$$\ln(N) = 5.768 - 2.030 \ln(\varepsilon_a - 0.126) + T^* \dot{\varepsilon}^* O^* \quad (7a)$$

and that of Type 316NG, as

$$\ln(N) = 6.913 - 1.671 \ln(\varepsilon_a - 0.126) + T^* \dot{\varepsilon}^* O^*, \quad (7b)$$

where the constants for transformed temperature, strain rate, and DO are defined as follows:

$$\begin{aligned} T^* &= 0 && (T < 200°C) \\ T^* &= 1 && (T \geq 200°C) \end{aligned} \quad (8a)$$

$$\begin{aligned} \dot{\varepsilon}^* &= 0 && (\dot{\varepsilon} > 0.4\%/s) \\ \dot{\varepsilon}^* &= \ln(\dot{\varepsilon}/0.4) && (0.0004 \leq \dot{\varepsilon} \leq 0.4\%/s) \\ \dot{\varepsilon}^* &= \ln(0.0004/0.4) && (\dot{\varepsilon} < 0.0004\%/s) \end{aligned} \quad (8b)$$

$$\begin{aligned} O^* &= 0.260 && (DO < 0.05 \text{ ppm}) \\ O^* &= 0.172 && (DO \geq 0.05 \text{ ppm}). \end{aligned} \quad (8c)$$

The model is recommended for predicted fatigue lives $\leq 10^6$ cycles. Recent test results indicate that for high–DO environments, conductivity of water is important for environmental effects on fatigue life of austenitic SSs. Therefore, the above correlations may be conservative for high–DO, i.e., ≥0.05 ppm DO, environments. The experimental values of fatigue life in air and water and those predicted from Eqs. 5–8 are plotted in Fig. 24. The estimated fatigue S–N curves for Types 304, 316, and 316NG SSs in air and LWR environments are shown in Figs. 5 and 25, respectively. The predicted fatigue lives show good agreement with the experimental data. Note that the ASME mean curve is not consistent with the existing fatigue S–N data (Fig. 5). Also, although the best–fit of the S–N data in LWR environments (Fig. 25) yields a steeper slope, the slope of the S–N curve in water was assumed to be the same as in air.

Upon completion of the modeling phase, the residual errors (i.e., the Cartesian distance from the prediction curve) should not show significant patterns, such as heteroskedasticity (changing variance), or a nonzero slope. The residual errors for each variable, grouped by steel type and environment (air or water), are plotted in Figs. 26–30. Most data subsets and plots

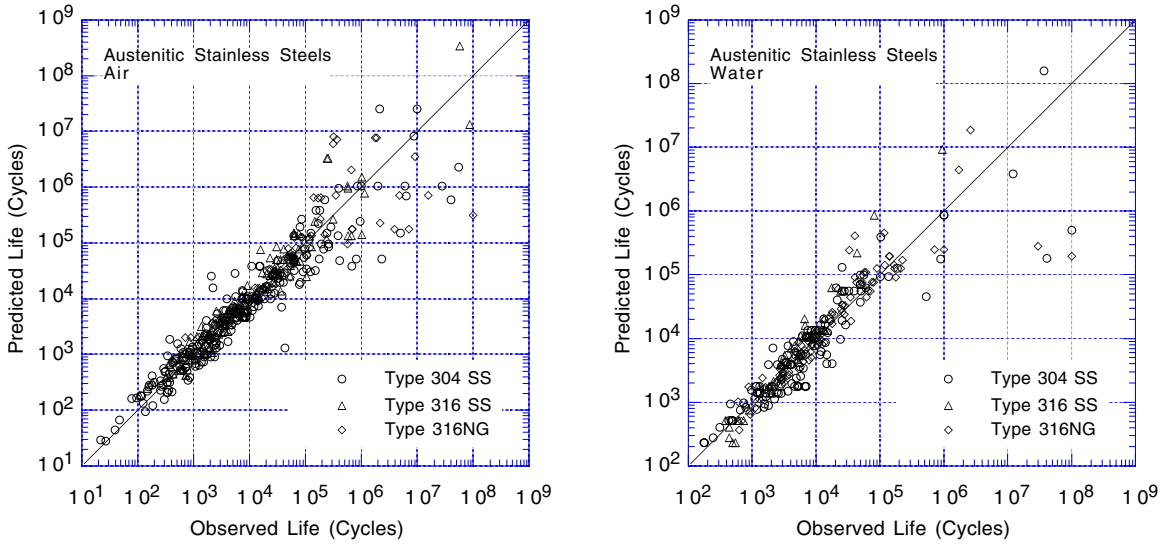

Figure 24. Experimental and predicted values of fatigue lives of austenitic SSs in air and water environments

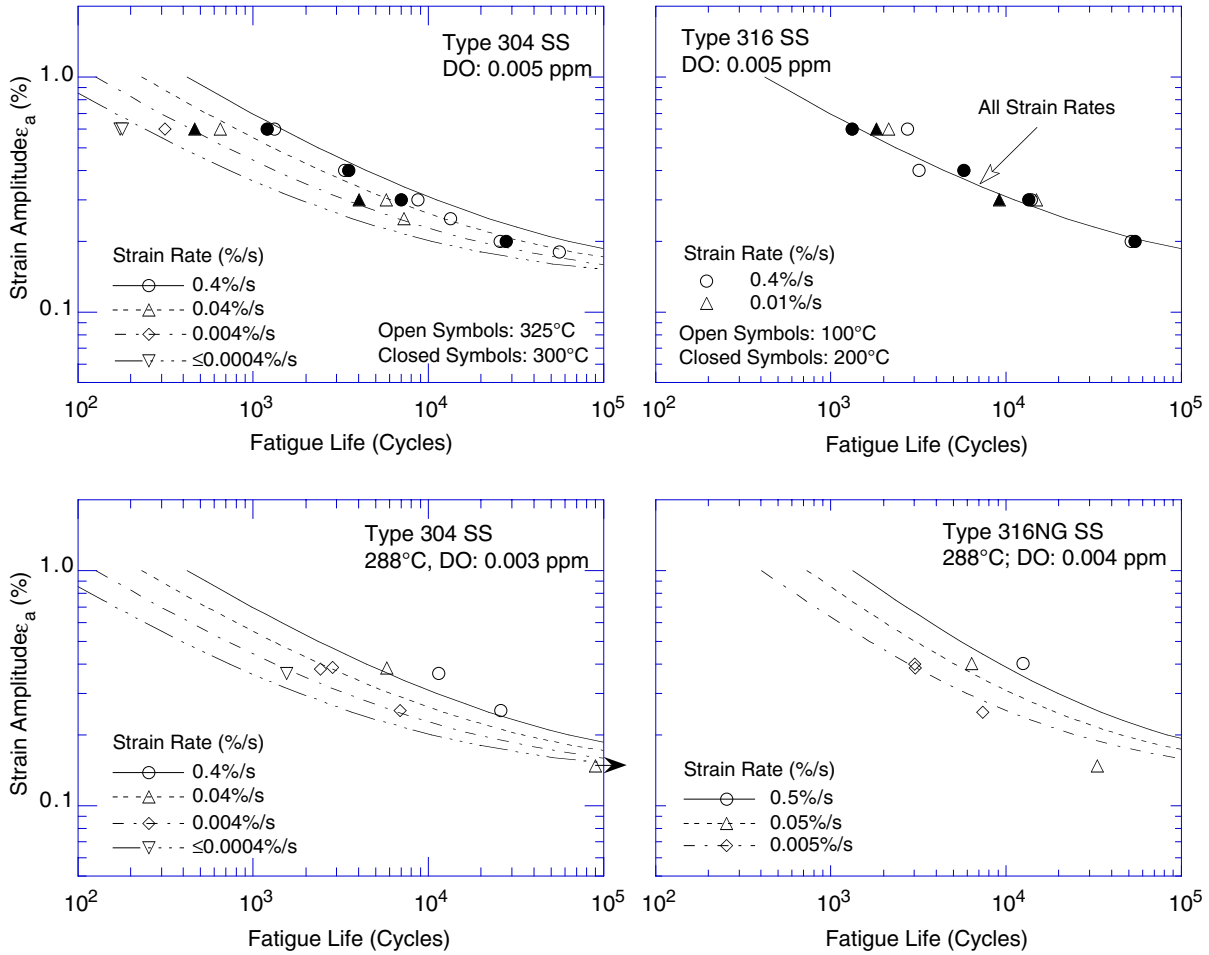

Figure 25. Experimental fatigue lives and those estimated from statistical models for austenitic SSs in water environments

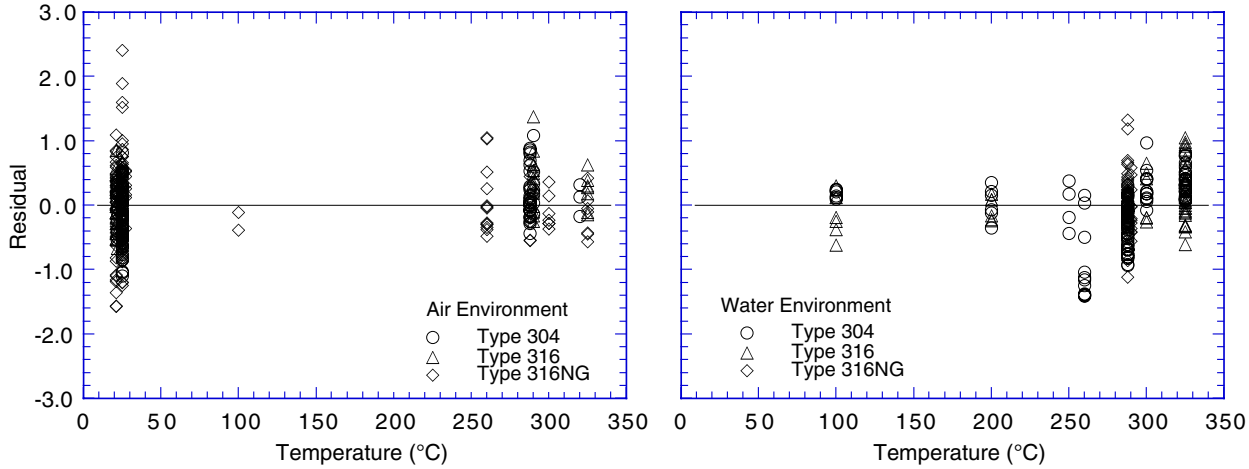

Figure 26. Residual error for austenitic SSs as a function of test temperature

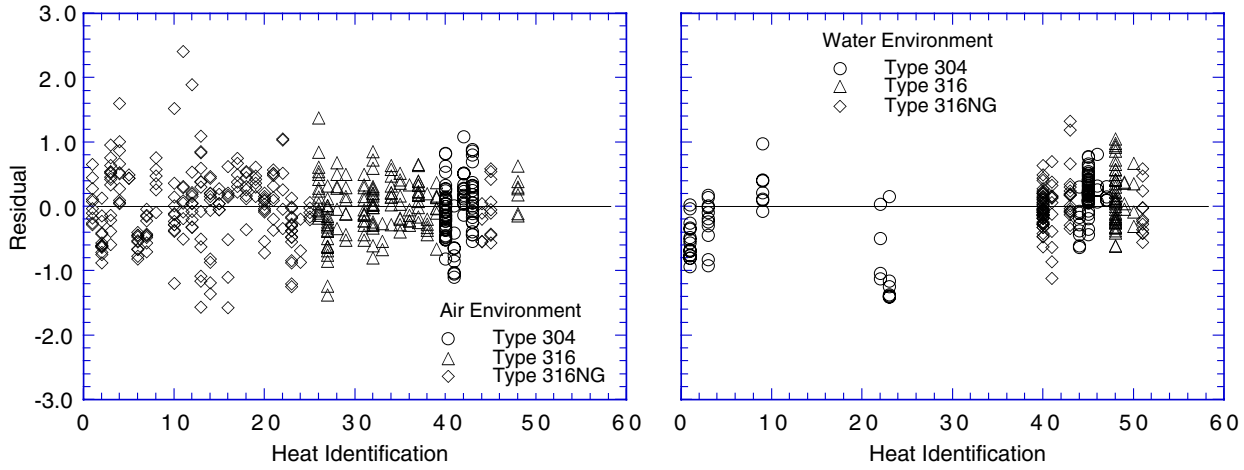

Figure 27. Residual error for austenitic SSs as a function of material heat

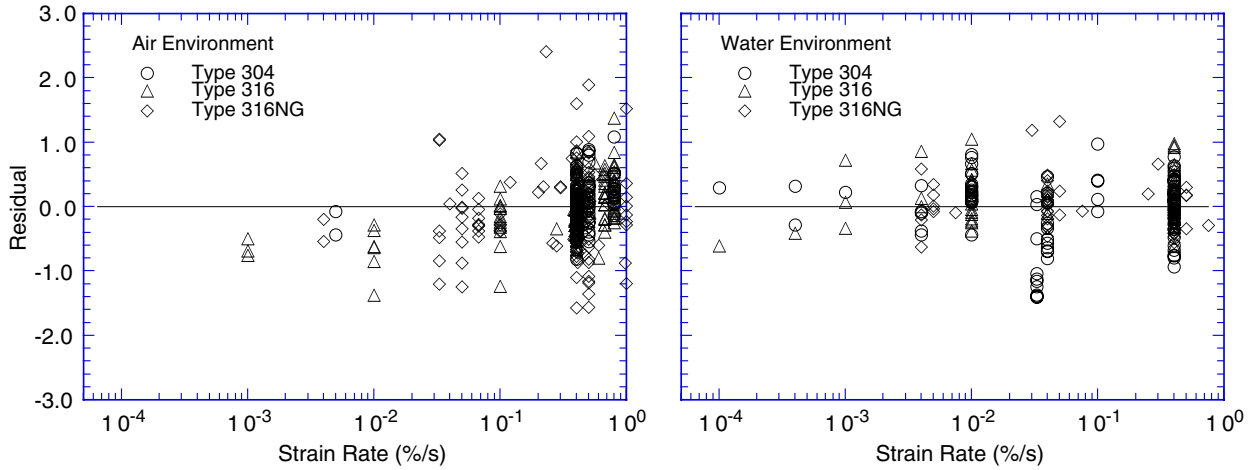

Figure 28. Residual error for austenitic SSs as a function of loading strain rate

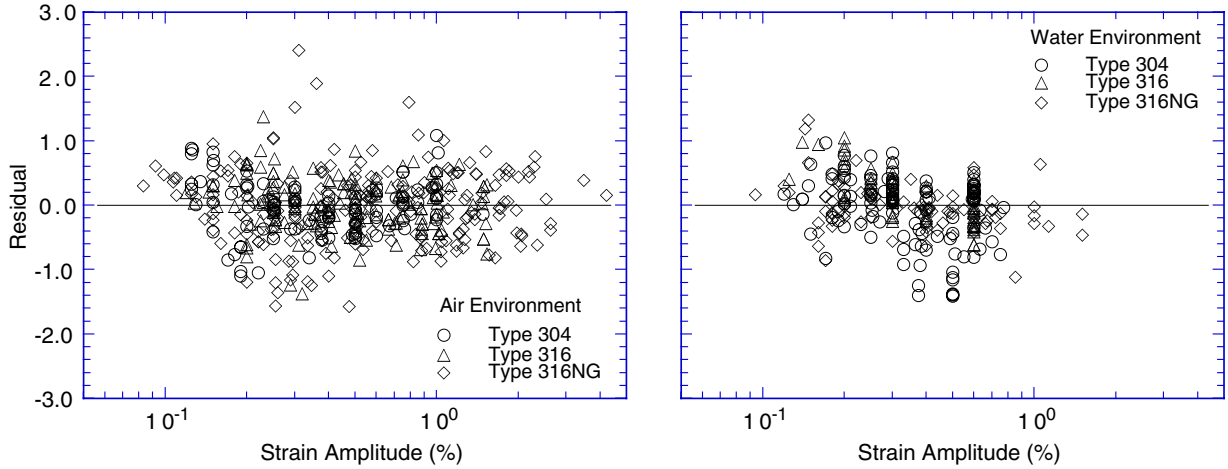

Figure 29. Residual error for austenitic SSs as a function of applied strain amplitude

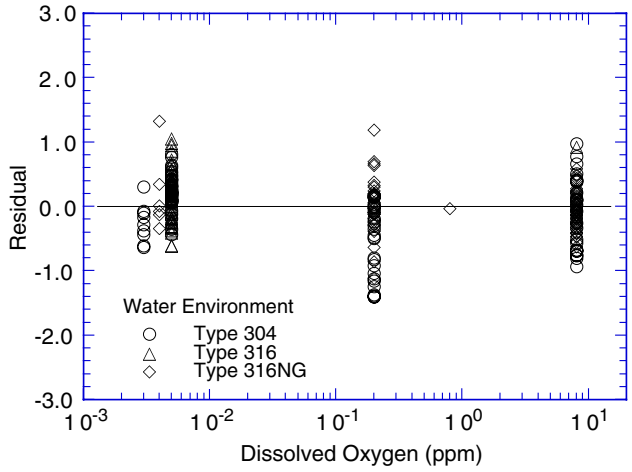

Figure 30.
Residual error for austenitic SSs as a function of dissolved oxygen in water

do not show patterns. In general, high variance tends to be associated with longer lives and lower strain amplitudes. Furthermore, biases seem to be traceable to heat–to–heat variation.

6 Design Fatigue Curves

The design fatigue curves in the current ASME Section III Code were based on experimental data on small polished test specimens. The curves were obtained by adjusting the best–fit curve for the effect of mean stress and then lowering the adjusted curve by a factor of 2 on stress or 20 on life, whichever was more conservative, at each point of the curve. The best–fit curve to the experimental data,[51] expressed in terms of strain amplitude ε_a (%) and fatigue cycles N, for austenitic SSs is given by

$$\ln[N] = 6.954 - 2.0 \ln(\varepsilon_a - 0.167). \quad (9)$$

The mean curve, expressed in terms of stress amplitude S_a (MPa), which is the product of ε_a and elastic modulus E, is given by

$$S_a = 58020/(N)^{1/2} + 299.92. \quad (10)$$

The strain–vs.–life data were converted to stress–vs.–life curves by using the room–temperature value of 195.1 GPa (28300 ksi) for the elastic modulus. The best–fit curves were adjusted for the effect of mean stress by using the modified Goodman relationship[46]

$$S_a' = S_a\left(\frac{\sigma_u - \sigma_y}{\sigma_u - S_a}\right) \qquad \text{for } S_a < \sigma_y, \tag{10a}$$

and $$S_a' = S_a \qquad \text{for } S_a > \sigma_y, \tag{10b}$$

where S_a' is the adjusted value of stress amplitude, and σ_y and σ_u are yield and ultimate strengths of the material, respectively. The Goodman relationship assumes the maximum possible mean stress and typically gives a conservative adjustment for mean stress, at least when environmental effects are not significant. The design fatigue curves were then obtained by lowering the adjusted best–fit curve by a factor of 2 on stress or 20 on cycles, whichever was more conservative, to account for differences and uncertainties in fatigue life associated with material and loading conditions.

The same procedure has been used to develop design fatigue curves for LWR environments. However, because of the differences between the ASME mean curve and the best–fit curve to existing fatigue data (Fig. 5), the margin on strain for the current ASME Code design fatigue curve is closer to 1.5 than 2. Therefore, to be consistent with the current Code design curve, a factor of 1.5 rather than 2 was used in developing the design fatigue curves from the updated statistical models in air and LWR environments.

The design fatigue curves based on the statistical model for Types 304 and 316 SS in air and low– and high–DO water are shown in Figs. 31–33. A similar set of curves can be obtained for Type 316NG SS. Because the fatigue life of Type 316NG is superior to that of Types 304 or 316 SS, Figs. 31–33 may be used conservatively for Type 316NG SS. Also, as mentioned earlier, recent test results indicate that the conductivity of water is important for environmental effects on fatigue life of austenitic SSs in high–DO environments. Therefore, the design fatigue curves for Type 304 and 316 SS in water with ≥0.05 ppm DO (Fig. 33) may be conservative.

Although, in air at low stress levels, the differences between the current ASME Code design curve and the design curve obtained from the updated statistical model at temperatures <250°C have been reduced or eliminated by reducing the margin on stress from 2 to 1.5, significant differences still exist between the two curves. For example, at stress amplitudes >300 MPa, estimates of life from the updated design curve are a factor of ≈2 lower than those from the ASME Code curve. Therefore, the actual margins on stress and life for the current ASME Code design fatigue curve are 1.5 and 10, respectively, instead of 2 and 20.

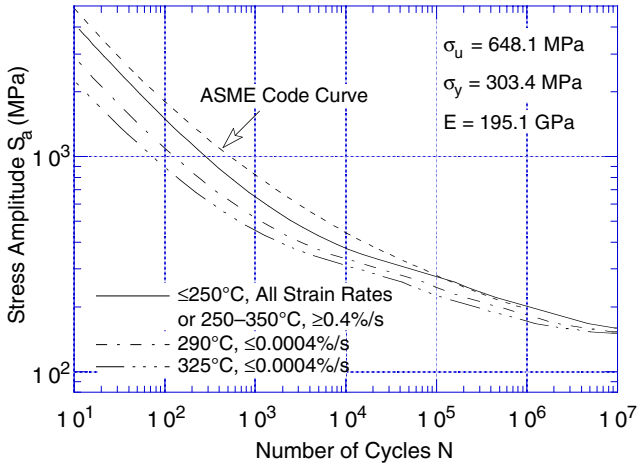

Figure 31.
ASME and statistical–model design fatigue curves for Types 304 and 316 SS in air

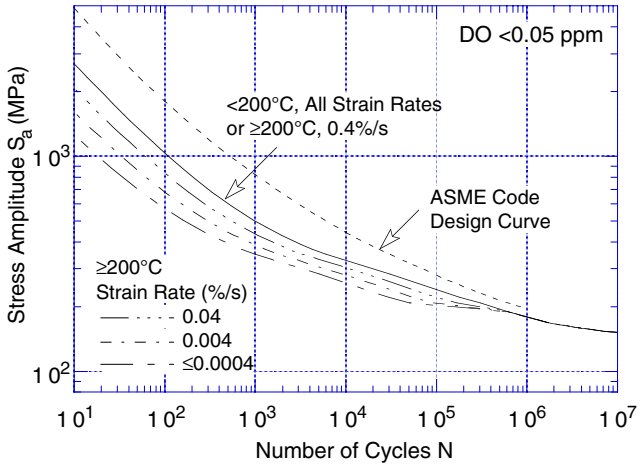

Figure 32.
ASME and statistical–model design fatigue curves for Types 304 and 316 SS in water with <0.05 ppm DO

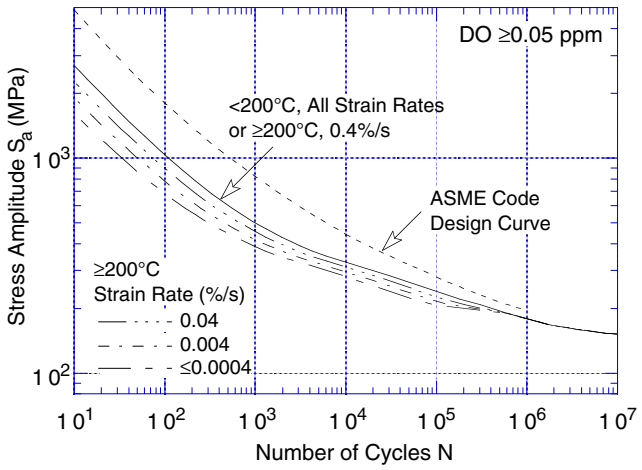

Figure 33.
ASME and statistical–model design fatigue curves for Types 304 and 316 SS in water with ≥0.05 ppm DO

As discussed above, the existing fatigue data indicate a threshold strain range of ≈0.32%, below which environmental effects on the fatigue life of austenitic SSs either do not occur or are insignificant. This value must be adjusted for the effects of mean stress and uncertainties due to material and loading variability. Threshold strain amplitudes are decreased by ≈10% to account for mean stress effects and by a factor of 1.5 to account for uncertainties in fatigue life associated with material and loading variability. Thus, a threshold strain amplitude of 0.097% (stress amplitude of 189 MPa) was selected, below which environmental effects on life are modest and are represented by the design curve for temperatures <200°C (shown by the solid line in Figs. 31 and 32).

These curves can be used to perform ASME Code fatigue evaluations of components that are in service in LWR environments. For each set of load pairs, a partial usage factor is obtained from the appropriate design fatigue curve. Information about the service conditions, such as temperature, strain rate, and DO level, are required for the evaluations. The procedure for obtaining these parameters depends on whether the elapsed–time–vs.–temperature information for the transient is available. The maximum values of temperature and DO level and the slowest strain rate during the transient may be used for a conservative estimate of life. Note that the design curves in LWR environments not only account for environmental effects on life but also include the difference between the current Code design curve and the updated design curve in air, i.e., the difference between the solid and dashed curves in Fig. 31.

7 Fatigue Life Correction Factor

The effects of reactor coolant environments on fatigue life have also been expressed in terms of a fatigue life correction factor F_{en}, which is the ratio of the life in air at room temperature to that in water at the service temperature.[11,52,53] To incorporate environmental effects into the ASME Code fatigue evaluation, a fatigue usage for a specific load pair, based on the current Code fatigue design curve, is multiplied by the correction factor. A fatigue life correction factor F_{en} can also be obtained from the statistical model, where

$$\ln(F_{en}) = \ln(N_{air}) - \ln(N_{water}). \quad (12)$$

From Eqs. 5a and 7a, the fatigue life correction factor relative to room–temperature air for Types 304 and 316 SSs is given by

$$F_{en} = \exp(0.935 - T^* \dot{\varepsilon}^* O^*), \quad (13)$$

where the threshold and saturation values for T^*, $\dot{\varepsilon}^*$, and O^* are defined in Eqs. 8a–8c. At temperatures ≥200°C and strain rates ≤0.0004%/s, Eq. 13 yields an F_{en} of ≈15 in low–DO PWR water (<0.05 ppm DO) and ≈8 in high–DO water (≥0.05 ppm DO). At temperatures <200°C, F_{en} is ≈2.5 in both low– and high–DO water at all strain rates.

8 Conservatism in Design Fatigue Curves

The overall conservatism in ASME Code fatigue evaluations has also been demonstrated in fatigue tests on piping welds and components.[54] In air, the margins on the number of cycles to failure for austenitic SS elbows and tees were 40–310 and 104–510, respectively. The margins for girth butt welds were significantly lower at 6–77. In these tests, fatigue life was expressed as the number of cycles for the crack to penetrate through the wall, which ranged in thickness from 6 to 18 mm (0.237 to 0.719 in). The fatigue design curves represent the number of cycles that are necessary to form a 3–mm–deep crack. Consequently, depending on wall thickness, the actual margins to failure may be lower by a factor of >2.

Deardorff and Smith[55] have discussed the types and extent of conservatisms present in the ASME Section III fatigue evaluations and the effects of LWR environments on fatigue margins. The sources of conservatism include design transients considerably more severe than those experienced in service, grouping of transients, and simplified elastic–plastic analysis. Environmental effects on two components, the BWR feedwater nozzle/safe end and PWR steam generator feedwater nozzle/safe end, both constructed from LAS and known to be affected by severe thermal transients,

were also investigated in the study. When environmental effects on fatigue life were not considered, Deardorff and Smith[55] estimated that the ratio of the CUFs for the PWR and BWR nozzles (both constructed from LAS), computed with the mean experimental curve for test specimen data, to CUFs computed with the Code fatigue design curve were ≈60 and 90, respectively. To maintain the factor of 20 on life that was used in the present Code fatigue design curves to account for the uncertainties due to material and loading variability, the margins for the PWR and BWR nozzles are reduced to 3 and 4.5, respectively. These results suggest that, for carbon and low–alloy steels, the Code Design procedures provide some margin in life that can be used to account for environmental effects on life. However, as noted previously in Section 6, the Code fatigue design curve for austenitic SSs is not consistent with the existing fatigue S–N data; the actual margins on stress and life are 1.5 and 10, respectively, instead of 2 and 20. Consequently, the Code fatigue design curve for austenitic SSs provides little or no margin in life to account for environmental effects.

Data available in the literature have been reviewed to evaluate the effects of various material, loading, and environmental variables on the fatigue life of structural materials in air and LWR environments.[33] The subfactors that may be used to account for the effects of these variables on fatigue life are summarized in Table 5. The factors on strain primarily account for variation in the fatigue limit of a material caused by material variability, component size and surface finish, and loading history. Because the reduction in fatigue life is associated with the growth of short cracks (<100 μm), the effects of these variables on threshold strain are typically not cumulative but rather are controlled by the variable that has the largest effect. The values in Table 5 suggest that a factor of at least 1.5 on strain and 10 on cycles is needed to account for the differences and uncertainties of relating the fatigue lives of laboratory test specimens to those of large components. Beacuse SSs develop a corrosion scale in LWR environments, the effect of surface finish may not be significant; the subfactor on life to account for surface finish effects may be as low as 1.5 or may be eliminated completely. Therefore, a factor of 1.5 or 2 on life may be able to account for the effects of environment on the fatigue lives of austenitic SSs.

Table 5. Subfactors that may be used to account for effects of various variables on fatigue life

Variable	Factor on Life	Factor on Strain
Material variability and experimental scatter	2.5	1.4–1.7
Size	1.4	1.25
Surface finish	2.0–3.0	1.3
Loading history	1.5–2.5	1.5
Total adjustment	10.0–26.0	1.5–1.7

9 Fatigue Evaluations in LWR Environments

Section III of the ASME Boiler and Pressure Vessel Code contains rules for the construction of nuclear power plant Class 1 components.[5] It provides requirements for designs that will withstand cyclic loadings on a structural component that occur because of changes in mechanical and thermal loadings as the system goes from one load set (pressure, temperature, moment, and force) to any other load set. ASME Section III, NB–3600 (piping design) methodology is used exclusively for piping and sometimes for branch nozzles. ASME Section III, NB–3200 (design by analysis) methodology is generally used for vessels and frequently for nozzles. In both cases, the various sets of load states at the most highly stressed locations in the component are defined first. The load states are defined in terms of the three principal stresses in NB–3200 methodology, and in terms of

internal pressure, moments, average temperature, and temperature gradients in NB–3600 methodology. A peak stress–intensity range and an alternating stress–intensity amplitude S_a is then calculated for each load state. The value of S_a is used to first obtain the allowable number of cycles from the design fatigue curve and then to calculate the fatigue usage associated with that load state. The CUF is the sum of the partial usage factors. The Section III, NB–3200– or NB–3600–type analyses of components for service in LWR environments can be performed with the design fatigue curves presented in Figs. 32 and 33. Note that fatigue evaluations performed with these updated curves not only account for the environmental effects but they also include the difference between the current ASME mean air curve and the statistical–model air curve.

An alternative approach to fatigue evaluations in LWR environments has been proposed by Electric Power Research Institute (EPRI)[52,53] and by the Environmental Fatigue Data (EFD) committee of Thermal and Nuclear Power Engineering Society (TENPES) of Japan.* As discussed in Section 7, the effects of LWR coolant environments on the fatigue S–N curves are expressed in terms of fatigue life correction factor F_{en}, defined as the ratio of the life in air at room temperature to that in water at service temperature. The effects of environment are incorporated into the ASME fatigue evaluation by obtaining a fatigue usage for a specific load pair based on the current Code design curves and multiplying it by the correction factor. Fatigue evaluations performed with the F_{en} incorporate only the effect of environment.

Both of these approaches require additional information about the service conditions, e.g., temperature, strain rate, and DO level. The procedure for obtaining these parameters depends on whether the elapsed–time–vs.–temperature information for the transient is available. The values of temperature and DO may be conservatively taken as the maximum values for the transient. An average strain rate is generally used for each load state; it is obtained from the peak strain and elapsed time for the transient. However, fatigue–monitoring data indicate that actual strain rates may vary significantly during the transient. The slowest strain rate can be used for a conservative estimate of life.

10 Summary

The work performed at ANL on fatigue of wrought and cast austenitic SSs in LWR environments is summarized. The existing fatigue S–N data have been evaluated to establish the effects of various material and loading variables, such as steel type, strain range, strain rate, temperature,and DO level in water on the fatigue lives of these steels. Current understanding of the fatigue S–N behavior of austenitc SSs may be summarized as follows.

10.1 Air Environment

- *Steel Type*: The fatigue lives of Types 304 and 316 SS are comparable; those of Type 316NG are superior. The fatigue S–N behavior of cast CF–8 and CF–8M SSs is similar to that of wrought austenitic SSs.
- *Temperature*: For all steels, life is independent of temperature in the range from room temperature to 427°C.
- *Strain Rate*: At temperatures above 260°C, the fatigue lives of austenitic SSs may decrease with decreasing strain rate.

---

*Presented at the Pressure Vessel Research Council Meeting, April 1996, Orlando, FL.

- *ASME Code Mean Curve*: The ASME mean curve for austenitic SSs is nonconservative with respect to existing fatigue S–N data; at strain amplitudes <0.5%, it predicts fatigue lives that are significantly longer than those observed experimentally.

10.2 LWR Environments

- *Environmental Effects*: The fatigue lives of cast and wrought austenitc SSs are decreased in LWR environments; the decrease depends on strain rate, DO level in water, and temperature.
- *Steel Type*: The effects of LWR environments on fatigue life are comparable for all steels.
- *Strain Amplitude*: A minimum threshold strain is required for environmentally assisted decrease in fatigue lives of the tested steels. The threshold value most likely corresponds to the rupture strain of the surface oxide film. Limited data suggest that the threshold strain is between 0.32 and 0.36%.
- *Loading Cycle*: Environmental effects on fatigue life occur primarily during the tensile–loading cycle, and at strain levels greater than the threshold value required to rupture the surface oxide film. Consequently, loading and environmental conditions, e.g., strain rate, temperature, and DO level, during the tensile–loading cycle in excess of the oxide rupture strain, are important parameters for environmentally assisted reduction in fatigue lives of the tested steels.
- *Dissolved Oxygen in Water*: Environmental effects on fatigue life are more pronounced in low–DO, i.e., <0.01 ppm DO, than in high–DO water, i.e., ≥0.1 ppm DO. The reduction in life is greater by a factor of ≈2 in a simulated PWR environment than in high–DO water. The fatigue lives of cast SSs are approximately the same in both high– or low–DO water and are comparable to those observed for wrought SSs in low–DO water. Recent data suggest that the fatigue lives of austenitic SSs may depend on parameters other than DO level in water, e.g., conductivity of water may be important.
- *Strain Rate*: Fatigue lives decrease with decreasing strain rate; the effect is greater in a low–DO PWR environment than in high–DO water. The results indicate that the strain rate below which effects of strain rate on fatigue life saturate may depend both on steel type and DO level. In low–DO PWR environments, saturation strain rate appears to be ≈0.0004%/s for Type 304 SS and somewhat higher for Type 316 SS.
- *Temperature*: Existing data are inadequate to establish the functional form for the dependence of life on temperature. Limited data indicate that environmental effects on fatigue life are significant at 250°C and minimal below 200°C. At 250–330°C, fatigue life appears to be relatively insensitive to changes in temperature.

10.3 Fatigue Design Curves in LWR Environments

Statistical models have been developed to predict fatigue life of small smooth specimens of austenitic SSs as a function of material, loading, and environmental parameters. Functional form and bounding values of these parameters were based on experimental observations and data trends. Statistical models were obtained by minimizing the squared Cartesian distances from the data point to the predicted curve instead of minimizing the sum of the square of the residual errors for either strain amplitude or fatigue life. The models are recommended for predicted fatigue lives of $\leq 10^6$ cycles. The results indicate that the ASME mean curve for SSs is not consistent with the

experimental data at strain amplitudes <0.5% or stress amplitudes <975 MPa (<141 ksi); the ASME mean curve is nonconservative.

The design fatigue curves for austenitic SSs in LWR environments were obtained by the procedure that was used to develop the current ASME Code design fatigue curves, i.e., by adjusting the best–fit experimental curve for the effect of mean stress and by setting margins of 20 on cycles and 2 on strain to account for the uncertainties in life associated with material and loading conditions. However, because the margin on strain for the current ASME Code design fatigue curve is closer to 1.5 than 2, a factor of 1.5 was used when the design fatigue curves in LWR environments were developed. Data available in the literature were reviewed to evaluate the conservatism in the existing Code fatigue design curves. The use of a fatigue life correction factor to incorporate the effects of environment into the ASME Code fatigue evaluations is also discussed.

References

1. K. Iida, *A Review of Fatigue Failures in LWR Plants in Japan*, Nucl. Eng. Des. **138**, 297–312 (1992).

2. K. Kussmaul, R. Rintamaa, J. Jansky, M. Kemppainen, and K. Törrönen, *On the Mechanism of Environmental Cracking Introduced by Cyclic Thermal Loading*, in IAEA Specialists Meeting Corrosion and Stress Corrosion of Steel Pressure Boundary Components and Steam Turbines, VTT Symp. 43, Espoo, Finland, pp. 195–243 (1983).

3. K. Kussmaul, D. Blind, and J. Jansky, *Formation and Growth of Cracking in Feed Water Pipes and RPV Nozzles*, Nucl. Eng. Des. **81**, 105–119 (1984).

4. E. Lenz, B. Stellwag, and N. Wieling, *The Influence of Strain Induced Corrosion Cracking on the Crack Initiation in Low Alloy Steels in HT–Water – A Relation Between Monotonic and Cyclic Crack Initiation Behavior*, in IAEA Specialists Meeting Corrosion and Stress Corrosion of Steel Pressure Boundary Components and Steam Turbines, VTT Symp. 43, Espoo, Finland, pp. 243–267 (1983).

5. *ASME Boiler and Pressure Vessel Code Section III – Rules for Construction of Nuclear Power Plant Components*, The American Society of Mechanical Engineers, New York (1992).

6. B. F. Langer, *Design of Pressure Vessels for Low–Cycle Fatigue*, ASME J. Basic Eng. **84**, 389–402 (1962) .

7. *Tentative Structural Design Basis for Reactor Pressure Vessels and Directly Associated Components (Pressurized, Water Cooled Systems)*, PB 151987, U.S. Dept. of Commerce, Office of Technical Service, 1 Dec. 1958 Revision.

8. S. Ranganath, J. N. Kass, and J. D. Heald, *Fatigue Behavior of Carbon Steel Components in High–Temperature Water Environments*, in BWR Environmental Cracking Margins for Carbon Steel Piping, EPRI NP–2406, Electric Power Research Institute, Palo Alto, CA, Appendix 3 (May 1982).

9. W. A. Van Der Sluys, *Evaluation of the Available Data on the Effect of the Environment on the Low Cycle Fatigue Properties in Light Water Reactor Environments*, in Proc. 6th Int. Symp. on Environmental Degradation of Materials in Nuclear Power Systems – Water Reactors, R. E. Gold and E. P. Simonen, eds., The Metallurgical Society, Warrendale, PA, pp. 1–4 (1993).

10. N. Nagata, S. Sato, and Y. Katada, *Low–Cycle Fatigue Behavior of Pressure Vessel Steels in High–Temperature Pressurized Water*, ISIJ Int. **31** (1), 106–114 (1991).

11. M. Higuchi and K. Iida, *Fatigue Strength Correction Factors for Carbon and Low–Alloy Steels in Oxygen–Containing High–Temperature Water*, Nucl. Eng. Des. **129**, 293–306 (1991).

12. M. Higuchi, K. Iida, and Y. Asada, *Effects of Strain Rate Change on Fatigue Life of Carbon Steel in High–Temperature Water*, in Fatigue and Crack Growth: Environmental Effects, Modeling Studies, and Design Considerations, PVP Vol. 306, S. Yukawa, ed., American Society of Mechanical Engineers, New York, pp. 111–116 (1995); also in Proc. of Symp. on Effects of the Environment on the Initiation of Crack Growth, ASTM STP 1298, American Society for Testing and Materials, Philadelphia (1997).

13. H. Kanasaki, M. Hayashi, K. Iida, and Y. Asada, *Effects of Temperature Change on Fatigue Life of Carbon Steel in High Temperature Water*, in Fatigue and Crack Growth: Environmental Effects, Modeling Studies, and Design Considerations, PVP Vol. 306, S. Yukawa, ed., American Society of Mechanical Engineers, New York, pp. 117–122 (1995).

14. G. Nakao, H. Kanasaki, M. Higuchi, K. Iida, and Y. Asada, *Effects of Temperature and Dissolved Oxygen Content on Fatigue Life of Carbon and Low–Alloy Steels in LWR Water Environment*, in Fatigue and Crack Growth: Environmental Effects, Modeling Studies, and Design Considerations, PVP Vol. 306, S. Yukawa, ed., American Society of Mechanical Engineers, New York, pp. 123–128 (1995).

15. O. K. Chopra and W. J. Shack, *Effects of LWR Environments on Fatigue Life of Carbon and Low–Alloy Steels*, in Fatigue and Crack Growth: Environmental Effects, Modeling Studies, and Design Considerations, PVP Vol. 306, S. Yukawa, ed., American Society of Mechanical Engineers, New York, pp. 95–109 (1995).

16. O. K. Chopra and W. J. Shack, *Evaluation of Effects of LWR Coolant Environments on Fatigue Life of Carbon and Low–Alloy Steels*, in Effects of the Environment on the Initiation of Crack Growth, ASTM STP 1298, W. A. Van Der Sluys, R. S. Piascik, and R. Zawierucha, eds., American Society for Testing and Materials, Philadelphia, pp. 247–266 (1997).

17. O. K. Chopra and W. J. Shack, *Low–Cycle Fatigue of Piping and Pressure Vessel Steels in LWR Environments*, Nucl. Eng. Des. **184**, 49–76 (1998).

18. O. K. Chopra and W. J. Shack, *Effects of LWR Coolant Environments on Fatigue Design Curves of Carbon and Low–Alloy Steels*, NUREG/CR–6583, ANL–97/18 (March 1998).

19. O. K. Chopra and W. J. Shack, *Fatigue Crack Initiation in Carbon and Low–Alloy Steels in Light Water Reactor Environments – Mechanism and Prediction*, in Fatigue, Environmental Factors, and New Materials, PVP Vol. 374, H. S. Mehta, R. W. Swindeman, J. A. Todd, S. Yukawa, M. Zako, W. H. Bamford, M. Higuchi, E. Jones, H. Nickel, and S. Rahman, eds., American Society of Mechanical Engineers, New York, pp. 155–168 (1998).

20. O. K. Chopra and W. J. Shack, *Overview of Fatigue Crack Initiation in Carbon and Low–Alloy Steels in Light Water Reactor Environments*, J. Pressure Vessel Technol. **121**, 49–60 (1999).

21. M. Fujiwara, T. Endo, and H. Kanasaki, *Strain Rate Effects on the Low Cycle Fatigue Strength of 304 Stainless Steel in High Temperature Water Environment, Fatigue Life: Analysis and Prediction*, in Proc. of the Int. Conf. and Exposition on Fatigue, Corrosion Cracking, Fracture Mechanics, and Failure Analysis, ASM, Metals Park, OH, pp. 309–313 (1986).

22. H. Mimaki, H. Kanasaki, I. Suzuki, M. Koyama, M. Akiyama, T. Okubo, and Y. Mishima, *Material Aging Research Program for PWR Plants*, in Aging Management Through Maintenance Management, PVP Vol. 332, I. T. Kisisel, ed., American Society of Mechanical Engineers, New York, pp. 97–105 (1996).

23. H. Kanasaki, R. Umehara, H. Mizuta, and T. Suyama, *Fatigue Lives of Stainless Steels in PWR Primary Water,* Trans. 14th Int. Conf. on Structural Mechanics in Reactor Technology (SMiRT 14), Lyon, France, pp. 473–483 (1997).

24. H. Kanasaki, R. Umehara, H. Mizuta, and T. Suyama, *Effects of Strain Rate and Temperature Change on the Fatigue Life of Stainless Steel in PWR Primary Water*, Trans. 14th Intl. Conf. on Structural Mechanics in Reactor Technology (SMiRT 14), Lyon, France, pp. 485–493 (1997).

25. M. Higuchi and K. Iida, *Reduction in Low–Cycle Fatigue Life of Austenitic Stainless Steels in High–Temperature Water,* in Pressure Vessel and Piping Codes and Standards, PVP Vol. 353, D. P. Jones, B. R. Newton, W. J. O'Donnell, R. Vecchio, G. A. Antaki, D. Bhavani, N. G. Cofie, and G. L. Hollinger, eds., American Society of Mechanical Engineers, New York, pp. 79–86 (1997).

26. M. Hayashi, *Thermal Fatigue Strength of Type 304 Stainless Steel in Simulated BWR Environment*, Nucl. Eng. Des. **184**, 135–144 (1998).

27. M. Hayashi, K. Enomoto, T. Saito, and T. Miyagawa, *Development of Thermal Fatigue Testing with BWR Water Environment and Thermal Fatigue Strength of Austenitic Stainless Steels*, Nucl. Eng. Des. **184**, 113–122 (1998).

28. W. J. Shack and W. F. Burke, *Fatigue of Type 316NG SS*, in Environmentally Assisted Cracking in Light Water Reactors, Semiannual Report, October 1989–March 1990, NUREG/CR–4667 Vol. 10, ANL–91/5, pp. 3–19 (March 1991).

29. O. K. Chopra and D. J. Gavenda, *Effects of LWR Coolant Environments on Fatigue Lives of Austenitic Stainless Steels*, in Pressure Vessel and Piping Codes and Standards, PVP Vol. 353, D. P. Jones, B. R. Newton, W. J. O'Donnell, R. Vecchio, G. A. Antaki, D. Bhavani, N. G. Cofie, and G. L. Hollinger, eds., American Society of Mechanical Engineers, New York, pp. 87–97 (1997).

30. O. K. Chopra and D. J. Gavenda, *Effects of LWR Coolant Environments on Fatigue Lives of Austenitic Stainless Steels*, J. Pressure Vessel Technol. **120**, 116–121 (1998).

31. O. K. Chopra and J. L. Smith, *Estimation of Fatigue Strain–Life Curves for Austenitic Stainless Steels in Light Water Reactor Environments*, in Fatigue, Environmental Factors, and New Materials, PVP Vol. 374, H. S. Mehta, R. W. Swindeman, J. A. Todd, S. Yukawa, M. Zako, W. H. Bamford, M. Higuchi, E. Jones, H. Nickel, and S. Rahman, eds., American Society of Mechanical Engineers, New York, pp. 249–259 (1998).

32. S. Majumdar, O. K. Chopra, and W. J. Shack, I*nterim Fatigue Design Curves for Carbon, Low–Alloy, and Austenitic Stainless Steels in LWR Environments*, NUREG/CR–5999, ANL–93/3 (April 1993).

33. J. Keisler, O. K. Chopra, and W. J. Shack, *Fatigue Strain–Life Behavior of Carbon and Low–Alloy Steels, Austenitic Stainless Steels, and Alloy 600 in LWR Environments*, NUREG/CR–6335, ANL–95/15 (Aug. 1995).

34. J. Keisler, O. K. Chopra, and W. J. *Shack, Statistical Models for Estimating Fatigue Strain–Life Behavior of Pressure Boundary Materials in Light Water Reactor Environments*, Nucl. Eng. Des. **167**, 129–154 (1996).

35. D. D. Macdonald, A. C. Scott, and P. Wentrcek, *External Reference Electrodes for Use in High Temperature Aqueous Systems*, J. Electrochem. Soc. **126**, 908–911 (1979).

36. C. E. Jaske, and W. J. O'Donnell, *Fatigue Design Criteria for Pressure Vessel Alloys*, Trans. ASME J. Pressure Vessel Technol. **99**, 584–592 (1977).

37. J. B. Conway, R. H. Stentz, and J. T. Berling, *Fatigue, Tensile, and Relaxation Behavior of Stainless Steels*, TID–26135, U.S. Atomic Energy Commission, Washington, DC (1975).

38. D. L. Keller, *Progress on LMFBR Cladding, Structural, and Component Materials Studies During July, 1971 through June, 1972, Final Report*, Task 32, Battelle–Columbus Laboratories, BMI–1928 (1977).

39. D. A. Hale, S. A. Wilson, E. Kiss, and A. J. Gianuzzi, *Low Cycle Fatigue Evaluation of Primary Piping Materials in a BWR Environment*, GEAP–20244, U.S. Nuclear Regulatory Commission (Sept. 1977).

40. C. Amzallag, P. Rabbe, G. Gallet, H. –P. Lieurade, *Influence des Conditions de Sollicitation Sur le Comportement en Fatigue Oligocyclique D'aciers Inoxydables Austénitiques*, Memoires Scientifiques Revue Metallurgie Mars 1978, pp. 161–173

41. A. Pellissier–Tanon, J. L. Bernard, C. Amzallag, and P. Rabbe, *Evaluation of the Resistance of Type 316 Stainless Steel Against Progressive Deformation*, in Low–Cycle Fatigue and Life Prediction, ASTM STP 770, C. Amzallag, B. N. Leis, and P. Rabbe, eds., American Society for Testing and Materials, Philadelphia, pp. 69–80 (1982).

42. Slama, G., Petrequin, P., and Mager, T., *Effect of Aging on Mechanical Properties of Austenitic Stainless Steel Castings and Welds*, in Assuring Structural Integrity of Steel Reactor Pressure Boundary Components, SMiRT Post Conference Seminar 6, Monterey, CA, 1983.

43. O. K. Chopra, *Effect of Thermal Aging on Mechanical Properties of Cast Stainless Steels*, in Proc. of the 2nd Int. Conf. on Heat–Resistant Materials, K. Natesan, P. Ganesan, and G. Lai, eds., ASM International, Materials Park, OH, pp. 479–485 (1995).

44. K. J. Miller, *Damage in Fatigue: A New Outlook*, in Pressure Vessels and Piping Codes and Standard: Volume 1 – Current Applications, PVP Vol. 313–1, K. R. Rao and Y. Asada, eds., American Society of Mechanical Engineers, New York, pp. 191–192 (1995).

45. S. Suresh and R. O. Ritchie, *Propagation of Short Fatigue Cracks*, Int. Metals Reviews **29**, 445–476 (1984).

46. K. Tokaji, T. Ogawa, and S. Osako, *The Growth of Microstructurally Small Fatigue Cracks in a Ferritic–Pearlitic Steel*, Fatigue Fract. Eng. Mater. Struct. **11**, 331–342 (1988).

47. D. J. Gavenda, P. R. Luebbers, and O. K. Chopra, *Crack Initiation and Crack Growth Behavior of Carbon and Low–Alloy Steels*, in Fatigue and Fracture 1, PVP Vol. 350, S. Rahman, K. K. Yoon, S. Bhandari, R. Warke, and J. M. Bloom, eds., American Society of Mechanical Engineers, New York, pp. 243–255 (1997).

48. K. Tokaji and T. Ogawa, *The Growth of Microstructurally Small Fatigue Cracks in Metals*, in Short Fatigue Cracks, ESIS 13, M. J. Miller and E. R. de los Rios, eds., Mechanical Engineering Publication, London, pp. 85–99 (1992).

49. F. P. Ford, *Overview of Collaborative Research into the Mechanisms of Environmentally Controlled Cracking in the Low Alloy Pressure Vessel Steel/Water System*, in Proc. 2nd Int. Atomic Energy Agency Specialists' Meeting on Subcritical Crack Growth, NUREG/CP–0067, MEA–2090, Vol. 2, pp. 3–71 (1986).

50. H. Hänninen, K. Törrönen, and W. H. Cullen, *Comparison of Proposed Cyclic Crack Growth Mechanisms of Low Alloy Steels in LWR Environments*, in Proc. 2nd Int. Atomic Energy Agency Specialists' Meeting on Subcritical Crack Growth, NUREG/CP–0067, MEA–2090, Vol. 2, pp. 73–97 (1986).

51. American Society of Mechanical Engineers, *Criteria of the ASME Boiler and Pressure Vessel Code for Design by Analysis in Sections III and VIII, Division 2*, ASME, New York (1969).

52. H. S. Mehta and S. R. Gosselin, *An Environmental Factor Approach to Account for Reactor Water Effects in Light Water Reactor Pressure Vessel and Piping Fatigue Evaluations*, EPRI Report TR–105759 (Dec. 1995).

53. H. S. Mehta and S. R. Gosselin, *An Environmental Factor Approach to Account for Reactor Water Effects in Light Water Reactor Pressure Vessel and Piping Fatigue Evaluations*, in Fatigue and Fracture Vol. 1, PVP 323, H. S. Mehta, ed., American Society of Mechanical Engineers, New York, pp. 171–185 (1996).

54. M. E. Mayfield, E. C. Rodabaugh, and R. J. Eiber, *A Comparison of Fatigue Test Data on Piping with the ASME Code Fatigue Evaluation Procedure*, ASME paper 79–PVP–92, American Society of Mechanical Engineers, New York (1979).

55. A. F. Deardorff and J. K. Smith, *Evaluation of Conservatisms and Environmental Effects in ASME Code, Section III, Class 1 Fatigue Analysis*, SAND94–0187, prepared by Structural Integrity Associates, San Jose, CA, under contract to Sandia National Laboratories (Aug. 1994).

NRC FORM 335 (2–89) NRCM 1102, 3201, 3202

U. S. NUCLEAR REGULATORY COMMISSION

BIBLIOGRAPHIC DATA SHEET

(See instructions on the reverse)

1. REPORT NUMBER *(Assigned by NRC. Add Vol., Supp., Rev., and Addendum Numbers, if any.)*
NUREG/CR–5704
ANL–98/31

2. TITLE AND SUBTITLE
Effects of LWR Coolant Environments on Fatigue Design Curves of Austenitic Stainless Steels

3. DATE REPORT PUBLISHED

MONTH	YEAR
March	1999

4. FIN OR GRANT NUMBER
W6610

5. AUTHOR(S)
O. K. Chopra

6. TYPE OF REPORT
Technical

7. PERIOD COVERED *(Inclusive Dates)*

8. PERFORMING ORGANIZATION – NAME AND ADDRESS *(If NRC, provide Division, Office or Region, U.S. Nuclear Regulatory Commission, and mailing address; if contractor, provide name and mailing address.)*

Argonne National Laboratory
9700 South Cass Avenue
Argonne, IL 60439

9. SPONSORING ORGANIZATION – NAME AND ADDRESS *(If NRC, type "Same as above": if contractor, provide NRC Division, Office or Region, U.S. Nuclear Regulatory Commission, and mailing address.)*

Engineering Issues Branch
Office of Nuclear Regulatory Research
U. S. Nuclear Regulatory Commission
Washington, DC 20555

10. SUPPLEMENTARY NOTES
M. McNeil, NRC Project Manager

11. ABSTRACT (200 words or less)

The ASME Boiler and Pressure Vessel Code provides rules for the construction of nuclear power plant components. Figures I–9.1 through I–9.6 of Appendix I to Section III of the Code specify fatigue design curves for structural materials. Although effects of reactor coolant environments are not explicitly addressed by the design curves, test data indicate that the Code fatigue curves may not always be adequate for coolant environments. This report summarizes work performed by Argonne National Laboratory on the fatigue of austenitic stainless steels in light water reactor (LWR) environments. Existing fatigue S–N data have been evaluated to establish the effects of various material and loading variables, such as steel type, dissolved oxygen level, strain range, strain rate, and temperature, on the fatigue lives of these steels. Statistical models are presented for estimating the fatigue S–N curves as a function of material, loading, and environmental variables. Design fatigue curves have been developed for austenitic stainless steel components in LWR environments. The extent of conservatism in the design fatigue curves and alternative methods for incorporating the effects of LWR coolant environments into the ASME Code fatigue evaluations are discussed.

12. KEY WORDS/DESCRIPTORS *(List words or phrases that will assist researchers in locating this report.)*
Fatigue Strain–Life Curves
Fatigue Design Curves
LWR Environments
Austenitic Stainless Steels
Cast Austenitic Stainless Steels
Fatigue Crack Initiation

13. AVAILABILITY STATEMENT
Unlimited

14. SECURITY CLASSIFICATION
(This Page)
Unclassified
(This Report)
Unclassified

15. NUMBER OF PAGES

16. PRICE

NRC FORM 335 (2–89)